construction engineering research laboratory

United States Army Corps of Engineers
...Serving the Army
...Serving the Nation

TECHNICAL REPORT M-272
October 1979

LEVEL II 12

INVESTIGATION OF RAPIDLY DEPLOYABLE PLASTIC FOAM SYSTEMS VOLUME II: NONLINEAR DEFORMATION AND LOCAL BUCKLING OF KEVLAR FABRIC/ POLYURETHANE FOAM COMPOSITES

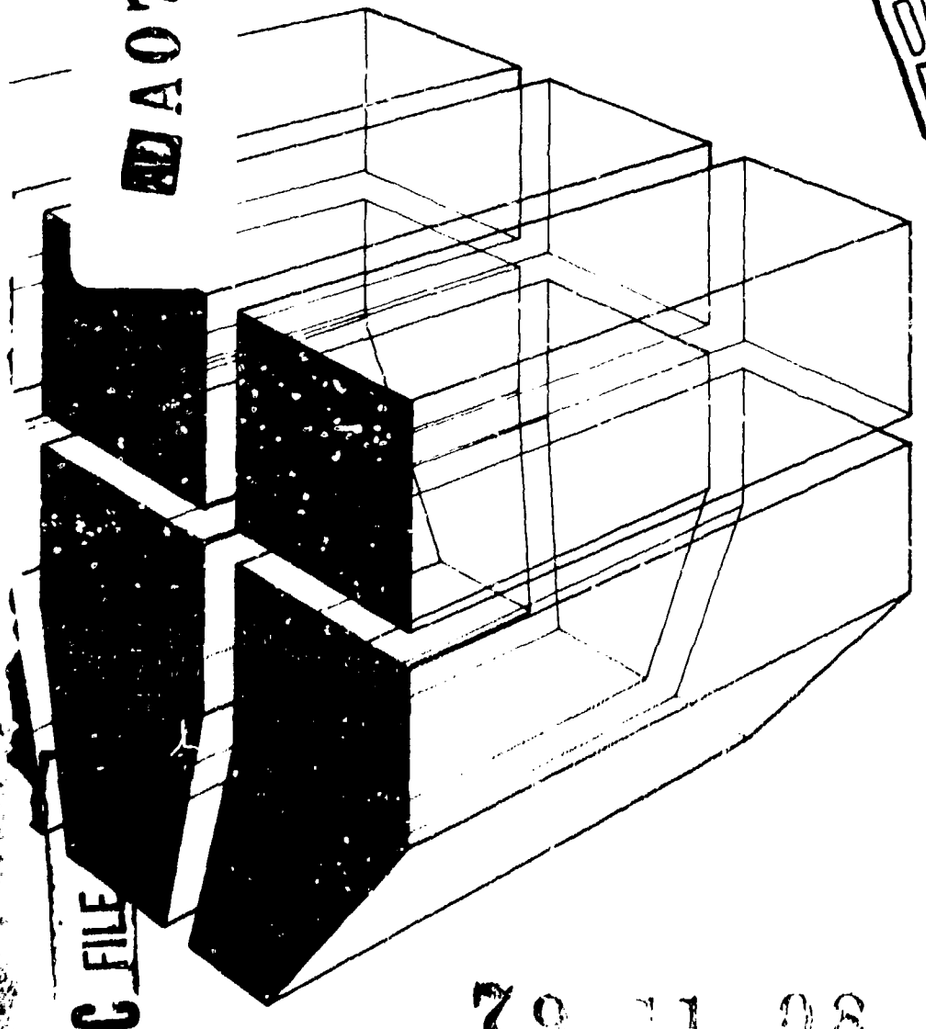

by
Alvin Smith
S. S. Wang
A. Y. Kuo

CERL

SECURITY CLASSIFICATION OF THIS PAGE (When Data Entered)

REPORT DOCUMENTATION PAGE

READ INSTRUCTIONS BEFORE COMPLETING FORM

1. REPORT NUMBER: CERL-TR-M-272—Vol.-2	2. GOVT ACCESSION NO.
3. RECIPIENT'S CATALOG NUMBER	
4. TITLE (and Subtitle): INVESTIGATION OF RAPIDLY DEPLOYABLE PLASTIC FOAM SYSTEMS. VOLUME II: NONLINEAR DEFORMATION AND LOCAL BUCKLING OF KEVLAR FABRIC/POLYURETHANE FOAM COMPOSITES.	5. TYPE OF REPORT & PERIOD COVERED: FINAL Rept
	6. PERFORMING ORG. REPORT NUMBER
7. AUTHOR(s): Alvin Smith, S. S. Wang, A. Y. Kuo	8. CONTRACT OR GRANT NUMBER(s): MIPR-FY1456-78-00006, MIPR-FY1456-79-00002
9. PERFORMING ORGANIZATION NAME AND ADDRESS: U.S. ARMY CONSTRUCTION ENGINEERING RESEARCH LABORATORY P.O. Box 4005, Champaign, IL 61820	10. PROGRAM ELEMENT, PROJECT, TASK AREA & WORK UNIT NUMBERS
11. CONTROLLING OFFICE NAME AND ADDRESS	12. REPORT DATE: October 1979
	13. NUMBER OF PAGES: 45
14. MONITORING AGENCY NAME & ADDRESS (if different from Controlling Office)	15. SECURITY CLASS. (of this report): Unclassified
	15a. DECLASSIFICATION/DOWNGRADING SCHEDULE

16. DISTRIBUTION STATEMENT (of this Report)

Approved for public release; distribution unlimited.

17. DISTRIBUTION STATEMENT (of the abstract entered in Block 20, if different from Report)

18. SUPPLEMENTARY NOTES

Copies are obtainable from National Technical Information Service
Springfield, VA 22151

19. KEY WORDS (Continue on reverse side if necessary and identify by block number)

foam
plastics
construction materials

20. ABSTRACT (Continue on reverse side if necessary and identify by block number)

Volume I of this report (1) presents the findings of a study conducted to develop a low-density polyurethane foam system that is deployable within 5 seconds, and (2) documents a study of foam/fabric cylinders as potential structural members. An especially fast-reacting foam formulation was devised, hardware for delivery and mixing of foam chemicals was designed and evaluated, various geometric shapes of constant volume that the foam could be formed into were investigated, and the impact loading characteristics of the foam at various times soon after generation were studied. Fabrication of fabric foam cylinders was also studied. Volume II of this report documents a

CONT

DD FORM 1 JAN 73 1473 EDITION OF 1 NOV 65 IS OBSOLETE

405 279

UNCLASSIFIED

SECURITY CLASSIFICATION OF THIS PAGE (When Data Entered)

Block 20 continued.

Cont → study of fabric-skinned, foam-filled cylindrical beams and an analytical/experimental study of their bending properties.

Results of the studies show that a low-density polyurethane foam system that will deploy within 5 seconds is practical to generate and to form into geometrically shaped lightweight fabric bags. The foam exhibits good impact absorption properties very quickly after formation; these properties can be used to attenuate rapidly applied loads of low to intermediate velocities. Finally, the fabric/foam composite beams possess interesting structural qualities commensurate with the fabric and foam used in making them. The analytical and experimental results compare very well. The analysis identified several factors of the mechanics involved that must be included in calculations to predict the loading response of such composites.

FOREWORD

This research was conducted for the Air Force Flight Dynamics Laboratory, Wright-Patterson Air Force Base, Dayton, OH. Funds were provided by Military Interdepartmental Purchase Request (MIPR) No. FY1456-78-00006 and MIPR No. FY1456-79-00002. The Air Force Project Manager was Mr. S. R. Mehaffie, AFFDL/FER.

The work was performed by the Engineering and Materials Division (EM), U.S. Army Construction Engineering Research Laboratory (CERL), Champaign, IL. The analysis of the fabric/foam cylinders was performed by Assistant Professor S. S. Wang and A. Y. Kuo of the Department of Theoretical and Applied Mechanics, University of Illinois at Urbana-Champaign. Dr. G. R. Williamson is Chief of EM.

COL Louis J. Circeo is Commander and Director of CERL and Dr. L. R. Shaffer is Technical Director.

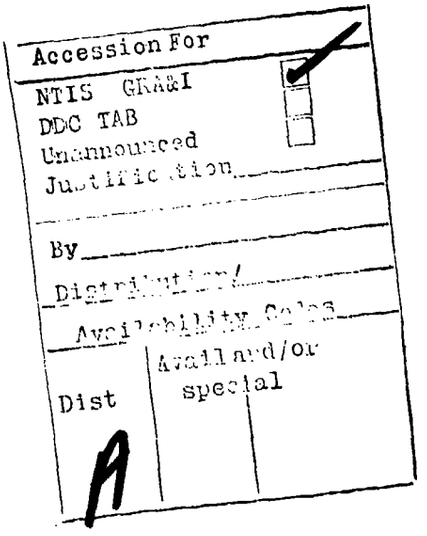

CONTENTS

FIGURES

FIGURES (cont'd)

FIGURES (cont'd)

INVESTIGATION OF RAPIDLY DEPLOYABLE PLASTIC FOAM SYSTEMS VOLUME II: NONLINEAR DEFORMATION AND LOCAL BUCKLING OF KEVLAR FABRIC/ POLYURETHANE FOAM COMPOSITES

1 INTRODUCTION

Background

Recent development of deployable, lightweight, high-strength composites has generated significant interest in their potential applications in aerospace structures, such as the ground impact attenuation system in the recovery technology of aerospace vehicles and in-orbit construction of large space structures[1]. The composite consists of a low-density fast-deployable structural foam as the core and a thin fabric/resin skin.

Extensive studies of several composite systems of this kind have been conducted by the Air Force Flight Dynamics Laboratory and the U.S. Army Construction Engineering Research Laboratory (CERL)[2]. Many diverse aspects of the material system have been thoroughly examined, ranging from the chemical formulation of polymer foams and fabrication processes of composites to prototype testing of composite structures. Fundamental concepts of fabrication, design, and testing of the composite structure have been reviewed.[3] The composite uses the most prominent properties of the fabric material and the space-filling foam, so that optimum performance may be achieved.

Recent development of strong aramid fibers has led to the selection of Kevlar* fabrics as one of the most promising candidates for the skin construction because of its excellent combination of mechanical, thermal, and corrosion-resistant properties. Advancement of the fast-foaming technology of high polymers for structural applications has made polyurethane a very attractive material for achieving the desired fabrication process and structural performance. In fact, it has been reported that, when proper mixing and injection are introduced, polyurethane foams can be deployed into a desired structural geometry within a few seconds.

Since the foam-filled, thin-skin composite structural members are constructed differently from those of conventional monolithic and fiber-reinforced composite materials, some fundamental difficulties have been encountered in the study of the behavior of the fabric/ foam composites. These include excessively large shear deformation of the section, local failure of the thin skin by wrinkling (or local buckling), and highly nonlinear response and creep behavior of the soft polyurethane foam core. These difficulties provide a great challenge in the design and analysis of the thin-skin, foam-filled composite structures and need to be fully investigated for future applications of the composite.

Objective

The overall objectives of this study were:

1. To reduce the operating time of a deployable plastic foam system to 5 seconds, to develop a mixing/ dispensing system for the foam, to evaluate a range of geometric shapes obtainable with the foam, and to evaluate the stress/strain characteristics of the foam at various times during the foam curing process.

2. To evaluate the performance of a high-strength fabric form filled with polyurethane foam to determine experimentally and analytically the roles of each component of the composite material as a potential structural material.

The objective of this volume is to present the experimental and analytical study of deformation and local failure of polyurethane foam-filled, thin Kevlar/ urethane skin composite cylinders subjected to transverse loading (four-point bending).

Approach

Chapter 2 describes the experimental procedure. In Chapter 3, methods of analysis for studying linear and nonlinear behavior of the composite cylinder are pre-

[1] T. Hagler, "Building Large Structures in Space," *Astronautics and Aeronautics*, Volume 14 (1976), pp 55-61; M. F. Card, "Trends in Aerospace Structures," *Astronautics and Aeronautics*, Volume 16 (1978), pp 82-89; S R. Mehaffie, "Foam Impact Attenuation System," to appear in *AIAA Proceedings* (1979).

[2] S. R. Mehaffie, *State of the Art of Impact Attenuation Concepts for RPV Applications*, AFFDL-TR-76-51 (WPAFB, 1976); S.R. Mehaffie, *Investigation of a Deployable Polyurethane Foam Ground Impact Attenuation System for Aerospace Vehicles (FIAS Tests # 1-48)*, AFFDL-TR-78-145, Volume I, (WPAFB, 1977); S. R. Mehaffie, *Investigation of a Deployable Polyurethane Foam Ground Impact Attenuation System for Aerospace Vehicles (FIAS Tests # 49-91)*, AFFDL-TR-78-145, Volume II (WPAFB, 1978); A. Smith, *Investigation of a Minimum Time Foam Deployment System*, draft Technical Report (CERL, 1979).

[3] S.R. Mehaffie, "Foam Impact Attenuation System," *A Collection of Technical Papers*, AIAA 6th Aerodynamic Decelerator and Balloon Technology Conference, Houston, TX, March 5-7, 1979.

*Dupont register trademark for Aramid fibers.

sented and the local buckling criterion during composite deformation is derived. Both pre-local-buckling and post-local-buckling responses of the beam are examined. Results obtained from the analyses are compared with experimental data and are given in Chapter 4. Their implications on the performance of the composites are discussed. Effects of different fabric/urethane skins and foam materials are studied. Emphasis is placed on determining the significance of transverse shear deformation and nonlinear core response after local buckling of the composite skin.

2 EXPERIMENTAL WORK

Design of the Experiment

Cylinders were selected for study since they represent the simplest structural shapes to make without the use of elaborate molds or forms. They can be tested in flexure to evaluate the function of each material component. It was recognized, however, that cylindrical beams are not optimum shapes in a structural sense.

Two high-strength fabrics were selected for the study. Both were woven of aramid fiber and coated with polyurethane elastomer to reduce porosity. The lightweight fabric was Kevlar 29 and the heavyweight fabric was Kevlar 49*. The aramids have a very high modulus of elasticity and high tensile strength.

Two densities of polyurethane foams were selected. A 2 lb/cu ft (32 kg/m^3) and a 4 lb/cu ft (64 kg/m^3) foam were to be used in combination with each fabric weight.

Two diameters of cylinders were used in the study. The original plan was to use 1- and 2-ft (0.3- and 0.6-m)-diameter beams to vary the beam section. When it was found that heat generated in the larger beams by the foam caused damage, 6-in. (0.15-m)-diameter cylinders were used.

Specimen Preparation

The cylinders were made by hand mixing preweighed batches of foam materials and pouring them into the sewn fabric forms. The expansion of the foam filled the forms. The seams of the forms were arranged so that they were along the sides of the beams and would not interfere with the loading. The top of each beam was identified so that load application would be parallel to the direction of rise of the foam.

*Kevlar 29 and Kevlar 49 are Dupont registered trademarks.

The beams were made without external formwork. The fabric skin defined the beam shape. In the case of the 1-ft (0.3-m)-diameter cylinders, the beams were very uniformly circular in cross section. The larger beams were somewhat elliptical, being about 4 in. (102 mm) less in height than width. The small (6 in. [0.15 m]) beams were circular in cross section.

The 1-ft (0.3-m)-diameter beams were made first. All the necessary material for the foam for each beam was mixed in a single batch and poured into the form at one end. The opening in the form for entry of the foam mixture was zippered so that it could be securely closed during the foaming process. A small air vent was provided in each end to allow air inside the form to escape. Two beams of each fabric weight and each foam weight were made.

The 2-ft (0.6-m)-diameter beams were made in the same manner as the 1-ft (0.3-m)-diameter beams, except half the required material was mixed and poured into each end of the fabric forms. The lower density foam beams were made first and the elliptical cross section mentioned previously was noted.

About 30 minutes after the end of foam expansion in the higher density foam beams, the first beam exploded. One seam was split completely from end to end and both circular end seams were split about two-thirds of the way around (Figure 1). Shortly before the explosion, internal temperature was noted to be at 375°F (190°C) and rising. The vast amount of heat generated could not escape and caused a combination of softening of the foam and thermal expansion of both the foam and the blowing agent within the cells. The use of the 2-ft (0.61-m)-diameter beams was abandoned because of the poor shape achieved and the excessive heat caused by the section thickness and quantity of foam being reacted. The ruptured beam showed extensive charring in the foam (Figure 2).

The 6-in. (0.15-m)-diameter beams were made without incident.

Testing

The beams were tested in flexure by a four-point loading method. The reaction points were placed 6 ft (1.83 m) apart and the two load points were evenly spaced 2 ft (0.61 m) apart and 2 ft (0.61 m) from the reaction points. Figure 3 shows the loading arrangement used with all of the test specimens.

Load spreading saddles were fabricated to use in the tests to prevent local crushing (Figure 4). The load bearing test set was designed to simulate an anticipated service loading case in which two cylinders would be in contact perpendicular to each other. The

Figure 1. Two-foot-diameter beam split open.

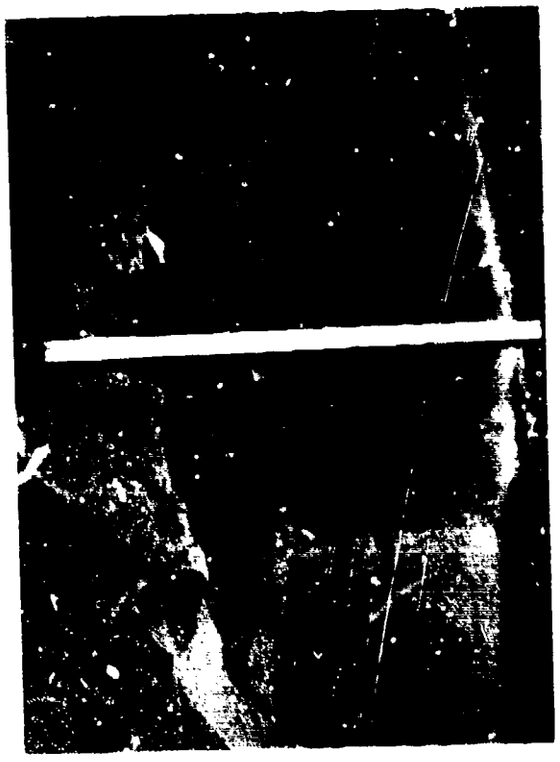

Figure 2. Charring of internal foam.

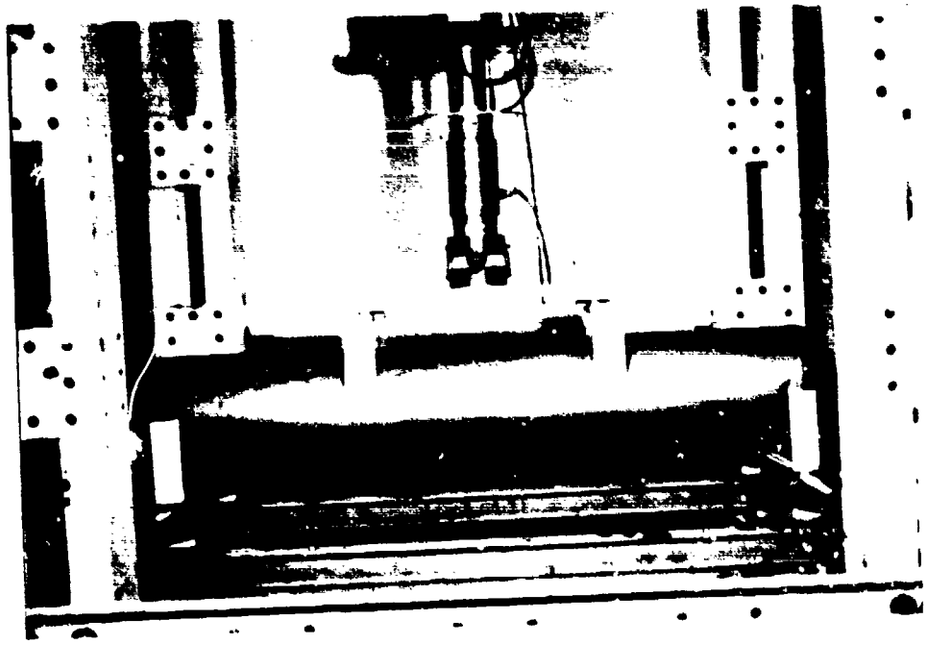

Figure 3. Test beam

Figure 4. Foam crushing by loading saddle.

saddles were 3 in. (76.2 mm) wide and conformed to the shape of the foam/fabric cylinders halfway around their circumference. There was some crushing of the foam by the saddles, especially in the lower density foam, but the effect was minimal. The effect of the saddles on the bending moment of the beams was considered negligible.

The equipment used in the test used a servoram with a 6-in. (0.15-m) travel. Strain gauges mounted on the fabric of the 1-ft (0.305-m)-diameter beams (Figures 5 and 6) failed to provide significant strain information. Ram stroke was recorded to provide deformation data. In all except one case, the beams bent to allow full ram travel. Figure 7 shows typical bending of a test beam. The lightweight fabric with the higher density foam failed by fracture within the "constant moment" portion of the beam between the load points.

3 FORMULATION OF ANALYSIS

The polyurethane foam-filled composite beam studied in this investigation is shown in Figure 8. The composite structure has a very intriguing combination of physical properties. It is light, stiff, strong, provides excellent impact resistance, and can be shaped efficiently. The skin is a thin-layer composite consist-

Figure 5. Strain gauge placement on beam.

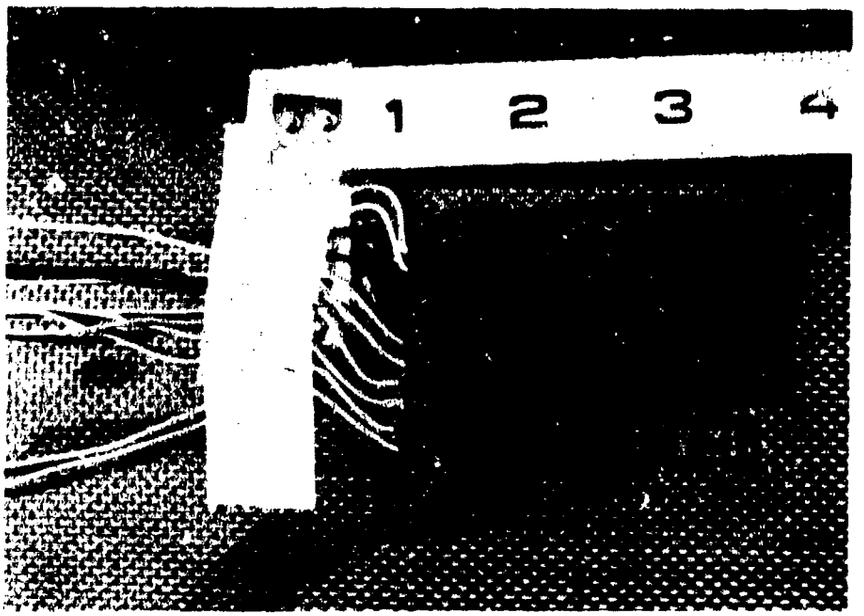

Figure 6. Strain gauge detail.

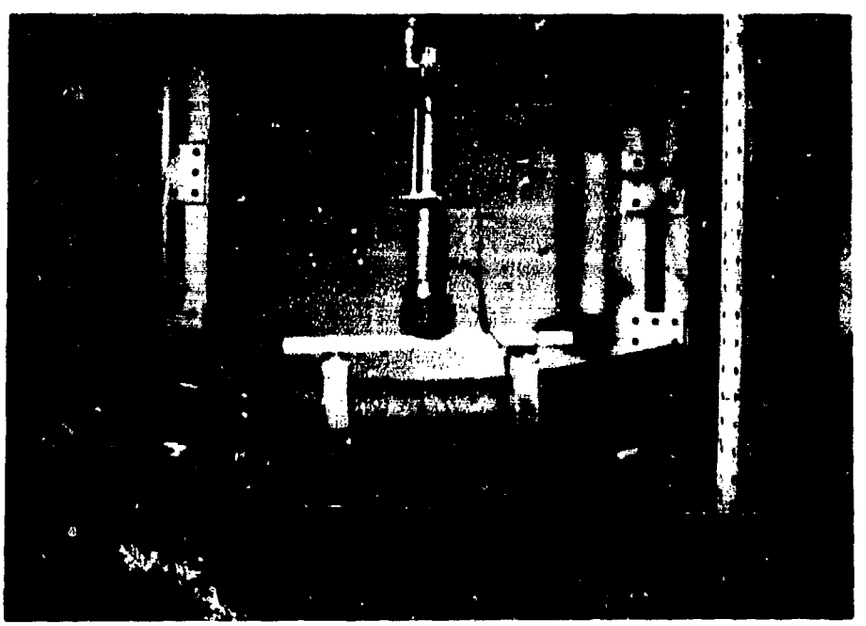

Figure 7. Bending of beam under load.

ing of high-strength Kevlar fabric and polyurethane resin. However, it has a relatively low resistance to compressive stresses and can lose its load-bearing capacity due to local buckling. The core is rather soft and deforms readily under stresses. Since the skin yields less readily than the core foam, almost all tensile and compressive forces initially are taken by the fabric/urethane skin; very little force is by the core, which acts predominantly in shear. As the external load increases, local buckling occurs in the compressive part of the skin. The core starts to take more and more compressive and shear stresses and deforms nonlinearly.

The major difference compared to the analysis and design of conventional structures is the need to account for the significant amount of shear deformation and the highly nonlinear response. Shear deformation in conventional structures is generally very small and is usually neglected, and properties of the materials are little affected by sustained load. In the foam-filled, thin-skin structures, not only is the shear deformation appreciable, but the nonlinearity of the core and the local buckling of the skin show tremendous effects on the load-bearing capacity of the composite. The analyses developed in this chapter are to take these effects into consideration and to provide a means of predicting the performance of the composite beam. It will be shown that in the nonlinear range of deformation, the situation is so complex that a numerical technique is required. The wrinkling load in the compressive region is derived to determine the local failure of the thin skin. Deformation of the composite beam after local buckling is further analyzed using a nonlinear finite element method.

Linear Analysis of Cylindrical Composite Beam Deformation

In the early state of loading, small deformation in the linear stress/strain range of the foam material is generally observed. Consider a differential element, dz, of the composite beam with a circular cross section as shown in Figure 8. The classical Kirchhoff's plane-remain-plane hypothesis is assumed in the composite beam deformation. The axial strain, ϵ, at any depth y from the central axis of the beam can be expressed by

$$\epsilon = \epsilon_o - \kappa y + \frac{d\beta}{dz} y \qquad \text{[Eq 1]}$$

where ϵ_o is the axial strain caused by stretching, κ is the curvature of the deformed central plane, $y = \theta$, and β is the angle of shear deformation of the plane. The neutral axis and the angle θ^* associated with the axis as shown in Figure 8 are, therefore, located at

$$y^* = \frac{\epsilon_o}{\kappa - \left(\frac{d\beta}{dz}\right)} = \frac{\epsilon_o}{\kappa^*} \qquad \text{[Eq 2a]}$$

and

$$\theta^* = \sin^{-1} \frac{y^*}{d_m} \qquad \text{[Eq 2b]}$$

where κ^* and d_m are defined as

$$\kappa^* = \kappa - \frac{d\beta}{dz} \quad \text{and} \quad d_m = \frac{1}{2}(d_o + d_i) \qquad \text{[Eq 3]}$$

in which d_i and d_o are the inner and outer radius of the skin in the composite, respectively.

The resultant axial force N and the resultant bending moment M acting on this section can be calculated by

$$\begin{aligned} N = &\int_{\theta^*}^{\pi-\theta^*} \int_{\frac{d_i}{2}}^{\frac{d_o}{2}} E_c^{(s)}(\epsilon_o - \kappa^* y)\, r\, dr\, d\theta \\ &+ \int_{\pi-\theta^*}^{2\pi-\theta^*} \int_{\frac{d_i}{2}}^{\frac{d_o}{2}} E_t^{(s)}(\epsilon_o - \kappa^* y)\, r\, dr\, d\theta \\ &+ \int_{y^*}^{\frac{d_i}{2}} E_c^{(f)}(\epsilon_o - \kappa^* y)\sqrt{d_i^2 - 4y^2}\, dy \\ &+ \int_{\frac{d_i}{2}}^{y^*} E_t^{(f)}(\epsilon_o - \kappa^* y)\sqrt{d_i^2 - 4y^2}\, dy \end{aligned} \qquad \text{[Eq 4]}$$

and

$$\begin{aligned} M = &\int_{\theta^*}^{\pi-\theta^*} \int_{\frac{d_i}{2}}^{\frac{d_o}{2}} E_c^{(s)}(\epsilon_o - \kappa^* y)\, y\, r\, dr\, d\theta \\ &+ \int_{\pi-\theta^*}^{2\pi+\theta^*} \int_{\frac{d_i}{2}}^{\frac{d_o}{2}} E_t^{(s)}(\epsilon_o - \kappa^* y)\, y\, r\, dr\, d\theta \\ &+ \int_{y^*}^{\frac{d_i}{2}} E_c^{(f)}(\epsilon_o - \kappa^* y)\, y \sqrt{d_i^2 - 4y^2}\, dy \\ &+ \int_{\frac{d_i}{2}}^{\frac{d_o}{2}} E_t^{(f)}(\epsilon_o - \kappa^* y)\, y \sqrt{d_i^2 - 4y^2}\, dy \end{aligned} \qquad \text{[Eq 5]}$$

where E is the Young's modulus, the superscripts (s) and (f) represent the modulus associated with the thin-skin composite layer and the foam core, respectively, and the subscripts c and t refer to the modulus in compression and tension, respectively.

Carrying out the integration in Eqs 4 and 5

$$N = C_{11}\,\epsilon_o + C_{12}\,\kappa^* \qquad \text{[Eq 6]}$$

$$M = C_{12}\,\epsilon_o + C_{22}\,\kappa^* \qquad \text{[Eq 7]}$$

where

$$C_{11} = \frac{\pi}{4} E_c^{(s)}(d_o^2 - d_i^2) + \frac{\pi}{8}(E_t^{(f)} + E_c^{(f)})\,d_i^2 + \frac{1}{4}(E_t^{(f)} - E_c^{(f)})\left(\sin^{-1}\frac{2y^*}{d_m} + \frac{2y^*}{d_m}\sqrt{1 - \frac{4y^{*2}}{d_i^2}}\right) \qquad \text{[Eq 8a]}$$

$$C_{22} = \frac{\pi}{64} E_c^{(s)}(d_o^4 - d_i^4) + \frac{1}{128}\pi d_i^4\,(E_t^{(f)} + E_c^{(f)}) + \frac{1}{32}(E_t^{(f)} - E_c^{(f)})\,d_i^4\left(\frac{1}{2}\sin^{-1}\frac{2y^*}{d_m} - \frac{y^*}{d_m}\sqrt{1 - \frac{4y^{*2}}{d_i^2}}\right) \qquad \text{[Eq 8b]}$$

and

$$C_{12} = \frac{1}{12}(E_t^{(f)} - E_c^{(f)})\,(d_i^2 - 4y^{*2})^{\frac{3}{2}} \qquad \text{[Eq 8c]}$$

It should be noted that bending and stretching are coupled in the composite beam deformation if the tensile and compressive moduli of the polyurethane foamed core are different. For simplicity without loss of generality, the foam is assumed to be isotropic in tension and compression; that is, if $E_c^{(f)} = E_t^{(f)} = E^{(f)}$, then the coupling effect disappears.

$$C_{11} = \frac{\pi}{4}\left[E^{(f)}\,d_i^2 + E^{(s)}\,(d_o^2 - d_i^2)\right] \qquad \text{[Eq 8a]}$$

$$C_{22} = \frac{\pi}{64}\left[E^{(f)}\,d_i^4 + E^{(s)}\,(d_o^4 - d_i^4)\right] \qquad \text{[Eq 8b]}$$

and

$$C_{12} = 0 \qquad \text{[Eq 8c]}$$

Using the fundamental beam equation, the resultant shear force V acting on a cross section can be obtained by

$$V = \frac{dM}{dz} \qquad \text{[Eq 9]}$$

The shear deformation of the composite beam may be evaluated by considering that all the shear force is taken by the core, since the cross-sectional area of the thin composite skin is much smaller than that of the core ($t/d_i \sim 0[10^{-3}]$).

$$\beta = -\frac{k}{G^{(f)}A}\frac{dM}{dz} \qquad \text{[Eq 10]}$$

where $G^{(f)}$ and A are the shear modulus and cross-sectional area of the foam core, respectively, and k is a conversion numerical factor having the value of 4/3 for a circular cross section as suggested by Mindlin.[4] Since the linear deformation of the composite beam w(z) can be related to bending moment M by

$$M = \kappa^* Z = \left(\frac{d^2w}{dz^2} - \frac{d\beta}{dz}\right)Z \qquad \text{[Eq 11]}$$

where Z is the bending rigidity of the composite beam defined as

$$Z = \frac{\pi}{64}\left[d_i^4\,E^{(f)} + (d_o^4 - d_i^4)E^{(s)}\right] \qquad \text{[Eq 12]}$$

for the case of $E_c^{(f)} = E_t^{(f)} = E^{(f)}$, the deflection of the beam can be directly obtained by integrating Eq 11

$$w(z) = \iint \frac{M}{Z}\,dz\,dz - \frac{16}{3\pi}\frac{M}{d_i^2 G^{(f)}} \qquad \text{[Eq 13]}$$

For a four-point bending problem of a circular cross-sectional composite beam as shown in Figure 9, the deflection w(z) can be calculated exactly as

$$w(z) = \begin{cases} \dfrac{PL^3}{Z}\left(\dfrac{z^2}{2L^2} - \dfrac{23}{24}\right) - \dfrac{16}{3\pi}\dfrac{PL}{d_i^2 G^{(f)}} & 0 \leqslant z \leqslant \dfrac{L}{2} \qquad \text{[Eq 14a]} \\ \dfrac{PL^3}{Z}\left(-\dfrac{z^3}{6L^3} + \dfrac{3z^2}{4L^2} - \dfrac{1}{8}\dfrac{z}{L} - \dfrac{15}{16}\right) - \dfrac{16}{3\pi}\dfrac{P(\frac{3}{2}L - z)}{d_i^2 G^{(f)}} & \dfrac{L}{2} \leqslant z \leqslant \dfrac{3}{2}L \qquad \text{[Eq 14b]} \end{cases}$$

Local Buckling (Wrinkling) of Composite Cylinders

When the thin-skin composite beam is subjected to bending and transverse loading, nonuniformly distributed axial compressive and tensile stresses occur

[4] R. D. Mindlin, "Influence of Rotatory Inertia and Shear on Flexual Motions of Isotropic Elastic Plates," *Journal of Applied Mechanics*, Volume 18 (1951), pp 31-38.

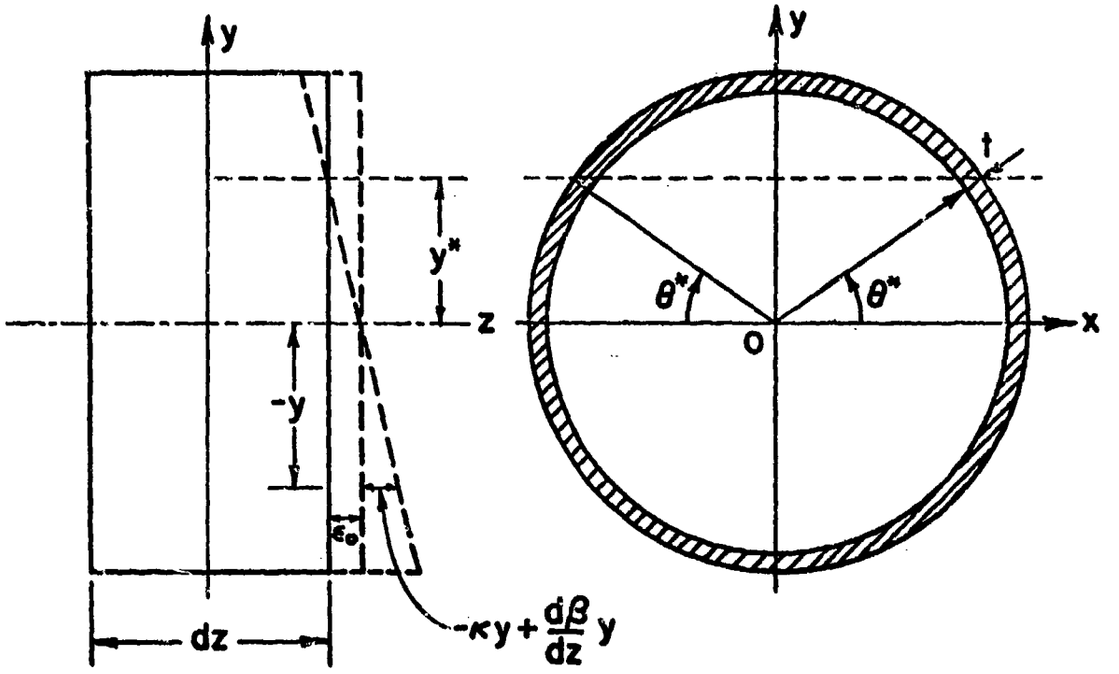

Figure 8. Deformation of an element of the deployable fabric/foam composite cylinder.

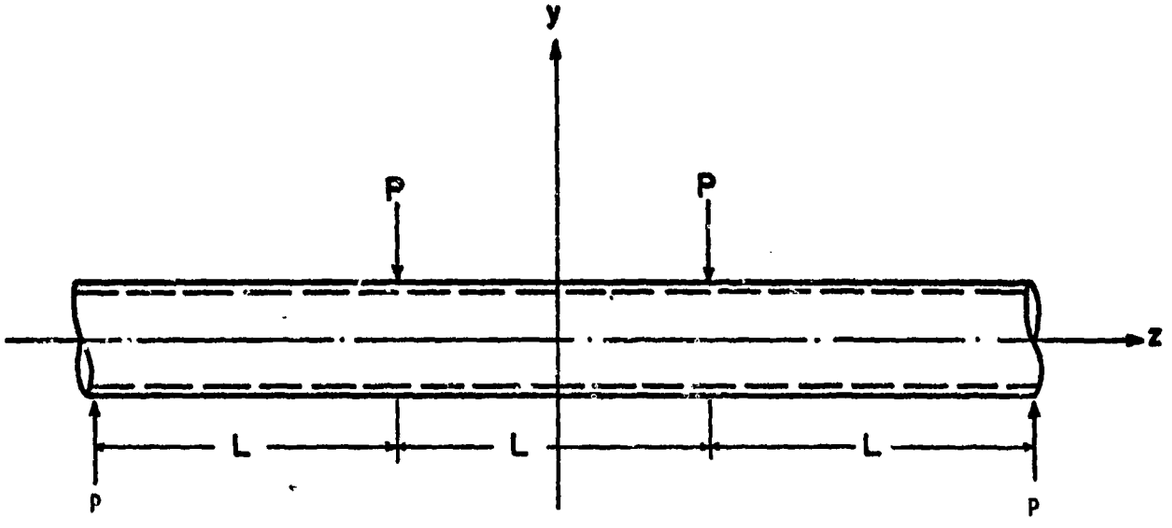

Figure 9. Deployable composite cylinder subjected to four-point bending.

in addition to transverse shear deformation. The axial compression and the transverse shear deformation in the composite may introduce local buckling (or wrinkling) of the composite skin in which the transverse normal stiffness may play an essential part. This local buckling phenomenon is a form of instability associated with short waves of skin deformation, which under a compressive load may be either symmetrical (out of phase) or antisymmetrical (in phase) with respect to the center plane of the core. The wrinkling is very pronounced and is of special importance for sandwich composite construction having a continuous low-density core material such as the soft polyurethane foam. Local buckling of the beam results in the loss of load-bearing capacity of a part of the thin composite skin under compression, while the overall structure is still capable of taking external loads. The load-carrying cross-sectional area of the composite member progressively reduces as the wrinkling in the Kevlar fabric/urethane skin develops when external loading increases continuously.

For a very thin-skin cylindrical composite beam ($t/d_i < 50$), the approximate method originally suggested in Williams[5] is applicable to the present problem. By evaluating the total potential energy of the system (i.e., bending energy of the skin, strain energy of the core associated with the normal and transverse shear stresses, and the potential energy of the external load) and using the standard minimization procedure for an elastic stability problem, the critical wrinkling stress σ_b can be obtained by[6]

$$\sigma_b \cong -0.76\,[G^{(f)}E^{(f)}E^{(s)}]^{\frac{1}{3}} \qquad \text{[Eq 15]}$$

Local buckling will occur and its effects should be considered in the deformation of the composite beam when maximum compressive stress in the beam, corresponding to an increasing external loading P_b, reaches this value.

Consider the present four-point bending problem of the composite beam as shown in Figure 9. Maximum bending occurs in the middle section of the span between $z = -L/2$ and $z = L/2$. The maximum compressive stress σ_{max} occurs at the point $\left(x = 0, y = \frac{d_o}{2}\right)$ of any section in the middle span and has the value

$$\sigma_{max} = E^{(s)}\left[\epsilon_o - \left(\kappa - \frac{d\beta}{dz}\right)\frac{d_o}{2}\right]. \qquad \text{[Eq 16]}$$

The pure bending condition in the midspan of the cylindrical beam implies

$$\frac{d\beta}{dz} = 0 \qquad \text{[Eq 17]}$$

and

$$\kappa = \frac{PL}{Z} \qquad \text{[Eq 18]}$$

Thus, the critical external force P_b at which local buckling of the composite skin occurs can be shown to have the following form

$$P_b \cong \frac{1.52Z}{Ld_oE^{(s)}}\,[G^{(f)}E^{(f)}E^{(s)}]^{\frac{1}{3}} \qquad \text{[Eq 19]}$$

Post-Local-Buckling Behavior of Cylindrical Composite Beams

When the composite beam is subjected to a four-point bending load, local buckling generally starts in the upper surface $\left(x = 0, y = \frac{d_o}{2}\right)$ of the filled cylinder, where the compressive stress is maximum and reaches the local buckling stress σ_b as discussed in the previous section. As the external load increases, a larger portion of the composite skin undergoes compressive stress exceeding σ_b; thus, the wrinkled area progressively increases. While local buckling in a composite skin continuously extends to a larger dimension, the nonwrinkled part of the section can still take further increasing loads. In the analysis of post-buckling deformation of the composite beam, it is convenient to divide the deformed cross section area into three distinct regions (Figure 10): (1) wrinkled portion in the skin ($y > y_b$), where load-bearing capacity of the skin has been lost entirely; (2) the active compressive region ($y_b > y > y^*$), where both the skin and the core are subjected to a compressive stress σ ($|\sigma| < |\sigma_b|$) with $E_c^{(s)} = E^{(s)}$ and $E_c^{(f)} = E^{(f)}$; and (3) the region under tensile stresses ($y < y_b$) where $E_t^{(s)} = E^{(s)}$ and $E_t^{(f)} = E^{(f)}$. The resultant axial force N and the resultant bending moment M can be evaluated

[5] D. Williams, *Sandwich Construction--A Practical Approach for the Use of Designers*, RAE Report No. Structures, 2, M. 2466 (1947).

[6] A. C. Eringen, "Buckling of a Sandwich Cylinder under Uniform Axial Compressive Loading," *Journal of Applied Mechanics*, Volume 18, No. 2 (1951), pp 195-202.

similarly to those in Eqs 4 and 5, except the first term in the right-hand side of Eq 4 is replaced by

$$2\int_{\theta^*}^{\theta_b}\int_{d_i/2}^{d_o/2} E^{(s)}(\epsilon_o - \kappa^* y)\, r\, dr\, d\theta$$

$$= \frac{E^{(s)}}{4}(\theta_b - \theta^*)(d_o^2 - d_i^2)\epsilon_o$$

$$+ \frac{E^{(s)}}{12}(d_o^3 - d_i^3)(\cos\theta_b - \cos\theta^*)\kappa^*$$

[Eq 20]

where

$$\theta_b = \sin^{-1}\left[\frac{y_b}{(d_i + d_o)/2}\right] \qquad \text{[Eq 21a]}$$

and

$$y_b = \left[\epsilon_o - \frac{\sigma_b}{E^{(s)}}\right]/\kappa^* \qquad \text{[Eq 21b]}$$

and the first term in the right-hand side of Eq 5 is replaced by

$$-2\int_{\theta^*}^{\theta_b}\int_{d_i/2}^{d_o/2} E^{(s)}(\epsilon_o - \kappa^* y)\, y\, r\, dr\, d\theta$$

$$= \frac{E^{(s)}}{12}(d_o^3 - d_i^3)(\cos\theta_b - \cos\theta^*)\epsilon_o$$

$$+ \frac{E^{(s)}}{64}(d_o^4 - d_i^4)[\theta_b - \theta^* - \frac{1}{2}(\sin 2\theta_b - \sin 2\theta^*)]\kappa^*$$

[Eq 22]

Thus, one obtains the following expressions:

$$N = C_{11}\,\epsilon_o + C_{12}\,\kappa^* \qquad \text{[Eq 23a]}$$

$$M = C_{21}\,\epsilon_o + C_{22}\,\kappa^* \qquad \text{[Eq 23b]}$$

where

$$C_{11} = \frac{E^{(s)}}{8}(d_o^2 - d_i^2)\left[\pi + 2\sin^{-1}\frac{2y_b}{d_m}\right]$$

[Eq 24a]

$$C_{12} = C_{21} = \frac{E^{(s)}}{12 d_m}(d_o^3 - d_i^3)(d_m^2 - 4y_b^2)^{\frac{1}{2}}$$

[Eq 24b]

$$C_{22} = \frac{\pi E^{(f)}}{64} d_i^4 + \frac{E^{(s)}}{64}(d_o^4 - d_i^4)$$

$$\left[\frac{\pi}{2} + \sin^{-1}\frac{2y_b}{d_m} - \frac{2y_b(d_m^2 - 4y_b^2)^{\frac{1}{2}}}{d_m^2}\right]$$

[Eq 24c]

Solving ϵ_o and κ^* from Eqs 23a and 23b, the post-buckling deflection w(x) of the cylindrical composite beam can be calculated by

$$w(x) = \int_0^{\tau}\int_0^{\xi} \kappa^*(\xi_1)\, d\xi_1\, d\xi$$

$$+ \begin{cases} \dfrac{-16\,PL}{3\pi d_i^2 G^{(f)}} & 0 \leq z \leq \dfrac{L}{2} \\[2ex] \dfrac{-16\,P(\frac{3}{2}L - z)}{3\pi d_i^2 G^{(f)}} & \dfrac{L}{2} \leq z \leq \dfrac{3}{2}L \end{cases}$$

[Eq 25]

It should be noted that nonlinear deformation of the soft core usually occurs after local buckling of the composite skin. Thus, the nonlinear constitutive relation of the core material should be included in the post-buckling analysis. A highly nonlinear governing differential equation is therefore obtained. It can be solved only by the numerical methods discussed in the next section.

Nonlinear Analysis of Cylindrical Composite Beam Deformation

The rigidity of polyurethane foam in the core is much smaller than that of the load-bearing Kevlar skin in the deployable composite structure. Core deformation in the foam-filled cylinder under transverse loading is observed generally deviating significantly from linearity, especially after local wrinkling of the skin starts. To understand the nonlinear behavior better and to obtain realistic quantitative results for design and comparison purposes (with experiments), it is necessary to include the post-yielding behavior of the foam material in the study and to conduct a nonlinear analysis of the problem. In the nonlinear range of composite deformation, governing differential equations become nonlinear and considerably more complicated than those of the linear case. Numerical methods such as the finite element analysis are preferable. Other complications, such as local failure of the skin by wrinkling and shear deformation can also be incorporated easily into the formulation.

Consider material nonlinearity of the foam by expressing its constitutive equation in a power law form as core deformation exceeds the yield strain

$$\sigma^{(f)} = \begin{cases} E^{(f)}\,\epsilon & |\epsilon| \leq 0.02 \\ A(\epsilon - 0.02)^n & \epsilon > 0.02 \\ -A(|\epsilon + 0.02|)^n & \epsilon < -0.02 \end{cases} \qquad \text{[Eq 26]}$$

where the coefficient A and the hardening exponent n can be determined from experiments. The Kevlar composite skin is assumed to deform linearly in both tension and compression until failure. Thus, the incremental skin and core stresses $\delta\sigma^{(s)}$ and $\delta\sigma^{(f)}$, can be written as

$$\delta\sigma^{(s)} = E^{(s)}\,(\delta\epsilon_o - y\,\delta\,\kappa^*) \qquad \text{[Eq 27]}$$

and

$$\delta\sigma^{(f)} = \begin{cases} E^{(f)}\,(\delta\epsilon_o - y\,\delta\,\kappa^*) & y_c \leq y \leq y_t \\ nA(\epsilon - 0.02)^{n-1}\,(\delta\epsilon_o - y\,\delta\,\kappa^*) & y_t < y < -\frac{d_i}{2} \\ -nA(|\epsilon + 0.02|)^{n-1}\,(\delta\epsilon_o - y\,\delta\,\kappa^*) & \frac{d_i}{2} < y < y_c \end{cases}$$

[Eq 28]

where y_c and y_t are planes in a section at which local compressive or tensile strains reach its yield strain ($\epsilon_{ys} = \pm 0.02$). The corresponding incremental resultant force δN, bending moment δM, and shear force δv can be obtained by

$$\delta N = \int_A \delta\sigma\, dA \qquad \text{[Eq 29a]}$$

$$\delta M = \int_A -y\,\delta\sigma\, dA \qquad \text{[Eq 29b]}$$

and

$$\delta V = \frac{3}{4} G^{(f)}\, A\, \delta\beta \qquad \text{[Eq 29c]}$$

Incremental Element Stiffness Matrix Formulation

In the formulation of the nonlinear finite element analysis of composite beam deformation–consider a cylindrical beam element (Figure 11) subjected to incremental loading–the stress/strain relation can be written as

$$\begin{Bmatrix} \delta N \\ \delta M \\ \delta V \end{Bmatrix} = \begin{bmatrix} C_{11} & C_{12} & 0 \\ C_{21} & C_{22} & 0 \\ 0 & 0 & C_{33} \end{bmatrix} \begin{Bmatrix} \delta\epsilon_o \\ \delta\kappa^* \\ \delta\beta \end{Bmatrix} \qquad \text{[Eq 30a]}$$

or

$$\delta\underset{\sim}{Q} = \underset{\sim}{C}\,\delta\underset{\sim}{\epsilon} \qquad \text{[Eq 30b]}$$

where

$$C_{11} = \frac{1}{8} E^{(s)} (d_o^2 - d_i^2)\left(\pi + 2\sin^{-1}\frac{2y_b}{d_m}\right) + \int_{y_t}^{y_c} E^{(f)} \sqrt{d_i^2 - 4y^2}\, dy + \int_{-\frac{d_i}{2}}^{y_t} nA(\epsilon - 0.02)^{n-1} \sqrt{d_i^2 - 4y^2}\, dy - \int_{y_c}^{\frac{d_i}{2}} nA(|\epsilon + 0.02|)^{n-1} \sqrt{d_i^2 - 4y^2}\, dy \qquad \text{[Eq 31a]}$$

$$C_{12} = C_{21} = \frac{1}{12 d_m} E^{(s)} (d_o^3 - d_i^3) \sqrt{d_m^2 - 4y_b^2} - \int_{-\frac{d_i}{2}}^{y_t} nA(\epsilon - 0.02)^{n-1} y \sqrt{d_i^2 - 4y^2}\, dy + \int_{y_c}^{\frac{d_i}{2}} nA(|\epsilon + 0.02|)^{n-1} y \sqrt{d_i^2 - 4y^2}\, dy \qquad \text{[Eq 31b]}$$

$$C_{22} = \frac{1}{64} E^{(s)} (d_o^4 - d_i^4)\left(\frac{\pi}{2} + \sin^{-1}\frac{2y_b}{d_m} - \frac{2y_b\sqrt{d_m^2 - 4y_b^2}}{d_m^2}\right) + \int_{y_t}^{y_c} E^{(f)} y^2 \sqrt{d_i^2 - 4y^2}\, dy + \int_{-\frac{d_i}{2}}^{y_t} nA(\epsilon - 0.02)^{n-1} \sqrt{d_i^2 - 4y^2}\, y^2\, dy - \int_{y_c}^{\frac{d_i}{2}} nA(|\epsilon + 0.02|)^{n-1} \sqrt{d_i^2 - 4y^2}\, y^2\, dy \qquad \text{[Eq 31c]}$$

and

$$C_{33} = \frac{3}{4} G^{(f)} A = \frac{3}{16} \pi d_i^2 G^{(f)} \qquad \text{[Eq 31d]}$$

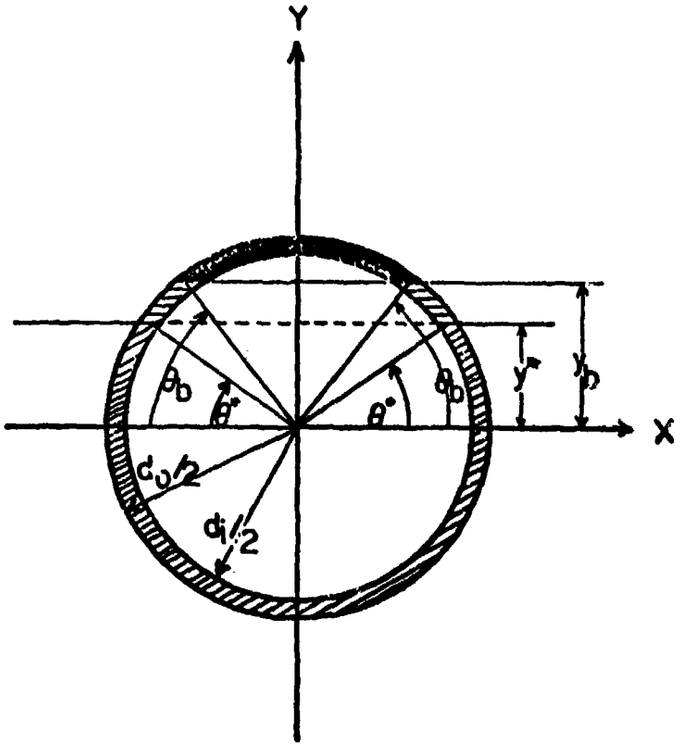

Figure 10. A cross section of locally buckled composite cylinder element.

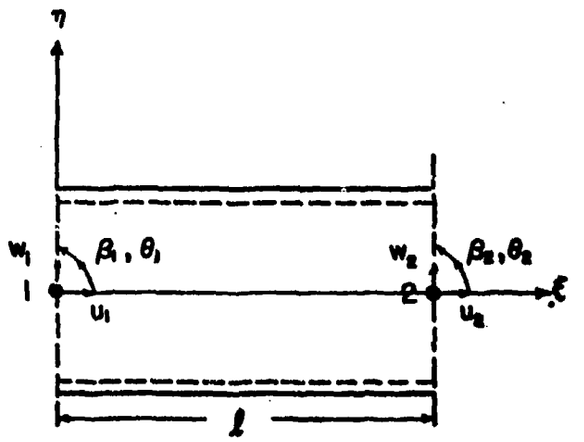

Figure 11. An element of deployable composite cylinder for nonlinear FEM analysis.

The strain-displacement equation, by definition, has the following form

$$\begin{Bmatrix} \epsilon_o \\ \kappa^* \\ \beta \end{Bmatrix} = \begin{bmatrix} \frac{d}{dz} & 0 & 0 \\ 0 & \frac{d^2}{dz^2} & -\frac{d}{dz} \\ 0 & 0 & 1 \end{bmatrix} \begin{Bmatrix} u \\ w \\ \beta \end{Bmatrix} \qquad \text{[Eq 32]}$$

or

$$\underset{\sim}{\epsilon} = \underset{\sim}{D}\underset{\sim}{q} \qquad \text{[Eq 33]}$$

where $\underset{\sim}{D}$ is a differential operator. Introducing interpolation functions (linear for u and β, and cubic for w), the displacement $\underset{\sim}{u}$ in an element may be expressed by element nodal displacements $\underset{\sim}{q}$

$$\begin{Bmatrix} u \\ w \\ \beta \end{Bmatrix} = \begin{bmatrix} (1-\xi) & 0 & 0 & 0 & \xi & 0 & 0 & 0 \\ 0 & (1-3\xi^2+2\xi^3) & \ell(1-\xi^2) & 0 & 0 & \xi^2(3-2\xi) & \ell(\xi^2-\xi) & 0 \\ 0 & 0 & 0 & (1-\xi) & 0 & 0 & 0 & \xi \end{bmatrix} \begin{Bmatrix} u_1 \\ w_1 \\ \theta_1 \\ \beta_1 \\ u_2 \\ w_2 \\ \theta_2 \\ \beta_2 \end{Bmatrix}$$

[Eq 34]

or

$$\underset{\sim}{u} = \underset{\sim}{R}\underset{\sim}{q} \qquad \text{[Eq 35]}$$

where $\xi = z/\ell$; ℓ is the length of the element; and u_i, w_i, i, β_i, ($i = 1,2$) are defined in Figure 11. Thus, one obtains

$$\underset{\sim}{\epsilon} = \underset{\sim}{B}\underset{\sim}{q} \qquad \text{[Eq 36]}$$

where

$$\underset{\sim}{B} = \underset{\sim}{D}\underset{\sim}{R} \qquad \text{[Eq 37]}$$

Following the routine procedure of the variational principle of minimum potential energy, the element stiffness matrix $\underset{\sim}{k}$ during an incremental loading step can be shown[7] to have the form

$$\underset{\sim}{\kappa} = \int_0^{\ell} \underset{\sim}{B}^T \underset{\sim}{C} \underset{\sim}{B} dz \qquad \text{[Eq 38]}$$

and the loading vector $\underset{\sim}{Q}$ is defined as

$$\underset{\sim}{Q}^T = [F_1, P_1, M_1, -M_1, F_2, P_2, M_2, -M_2]$$

[Eq 39]

where superscript T represents the transpose of the associated matrix, since the work done due to external loads is

$$W = F_1 u_1 + P_1 w_1 + M_1(0 - \beta_1) + F_2 u_2 + P_2 w_2 + M_2(0_2 - \beta_2) \qquad \text{[Eq 40]}$$

Eqs 38 and 39 are used directly in a mixed-mode solution procedure for the nonlinear analysis of the composite cylinder.

Step-Iteration Solution Scheme for Nonlinear Analysis

The present solution scheme uses a combination of incremental and iterative procedures for solving the material nonlinear problem. The overall procedure is shown graphically in Figures 12 and 13. The load is divided into many increments or partial loads and is applied one increment at a time as shown in Figure 12. Within each load increment, a tangent-stiffness iterative procedure[8] (Figure 13) is used to determine the true solution.

The final solution after n steps of increments is equal to the summation of all incremental solutions. This mixed-mode solution scheme can be described mathematically as the following. The load $\underset{\sim}{Q}_i$ after the application of the ith increment, is given by

$$\underset{\sim}{Q}_i = \underset{\sim}{Q}_o + \sum_{j=1}^{i} \Delta \underset{\sim}{Q}_j \qquad \text{[Eq 41]}$$

An increment to the displacements $\underset{\sim}{q}_i$ after nth iteration can be computed by

$$\underset{\sim}{K}_i^{(n)} \Delta \underset{\sim}{q}_i^{(n)} = (\underset{\sim}{Q}_{i+1} - \underset{\sim}{Q}_i) - \underset{\sim}{I}_i^{(n-1)} \qquad \text{[Eq 42]}$$

where $\underset{\sim}{I}_i^{(n-1)}$ is the load equilibrated after the previous cycle, and $\underset{\sim}{K}_i^{(n)}$, the stiffness of the nth cycle, is usually chosen by the tangent stiffness matrix at the end of the previous, i.e., the (n-1)th iterative step. Thus, Eq 42 becomes

$$\underset{\sim}{K}_i^{(n-1)} \Delta \underset{\sim}{q}_i^{(n)} = (\underset{\sim}{Q}_{i+1} - \underset{\sim}{Q}_i) - \underset{\sim}{I}_i^{(n-1)} \qquad \text{[Eq 42]}$$

Total displacements after nth iteration during a load increment $(\underset{\sim}{Q}_{i+1} - \underset{\sim}{Q}_i)$ are computed from

$$\underset{\sim}{q}_i^{(n)} = \underset{\sim}{q}_i^{(o)} + \sum_{m=1}^{n} \Delta \underset{\sim}{q}_i^{(m)} \qquad \text{[Eq 44]}$$

The current equilibrated load $\underset{\sim}{I}_i^{(n)}$ is evaluated as the load necessary to maintain the displacement $\underset{\sim}{q}_i^{(n)}$ by

$$\underset{\sim}{I}_i^{(n)} = \int_0^{\ell} \underset{\sim}{B}^T \underset{\sim}{C} \underset{\sim}{B} \underset{\sim}{q}_i \, dx \qquad \text{[Eq 45]}$$

This iterative procedure is repeated until the increments of displacements or unbalanced loads become zero, i.e., $\Delta \underset{\sim}{q}_i^{(n)}$ or $(\underset{\sim}{Q}_{i+1} - \underset{\sim}{Q}_i - \underset{\sim}{I}_i^n)$ sufficiently

[7] C. S. Desai and J. F. Abel, *Introduction to the Finite Element Method* (Van Nostrand Reinhold Company, 1972).

[8] C. S. Desai.

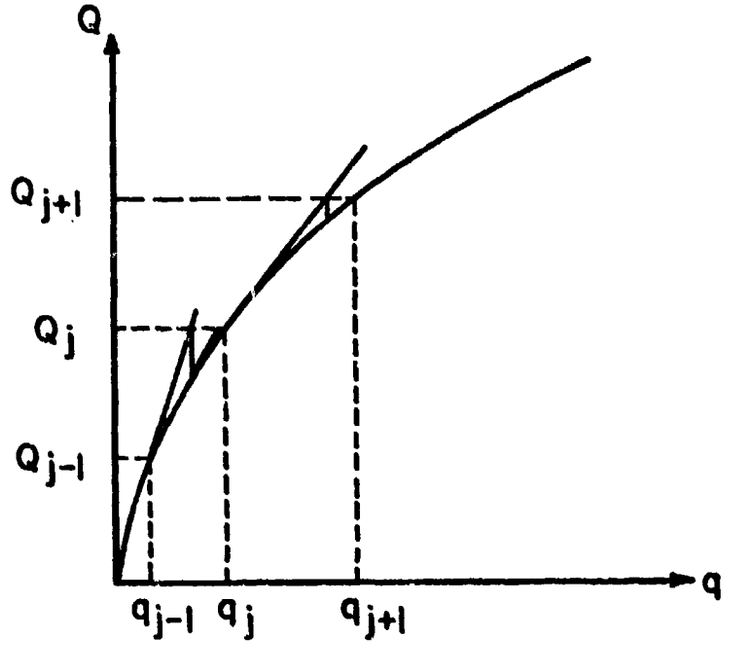

Figure 12. Step-iteration solution scheme.

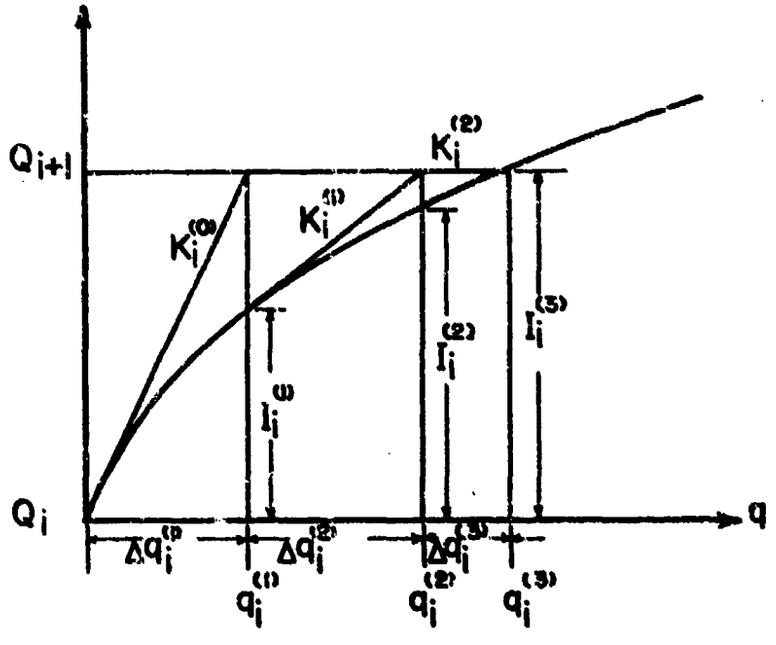

Figure 13. Tangent stiffness iterative solution procedure.

close to null according to some preset criterion. The total displacements after ith increments of loads are calculated by

$$\underset{\sim}{q}_i = \underset{\sim}{q}_0 + \sum_{j=1}^{i} \underset{\sim}{q}_j \qquad \text{[Eq 46]}$$

Then additional incremental load $(\underset{\sim}{Q}_{i+1} - \underset{\sim}{Q}_{i+1})$ is added and the similar procedure is repeated until the applied load level is reached.

4 MECHANICAL PROPERTIES OF FABRIC/URETHANE COMPOSITE SKIN AND POLYURETHANE FOAMS

High modulus, high-strength Kevlar aramid fibers offer an extremely desirable performance which is well suited to the construction of a wide range of engineering components and structures using advanced fiber-reinforced composites. The use of Kevlar fibers in the form of fabrics and fabric composites has been relatively new. Fabrics of the Kevlar aramid have been found to possess similarly attractive properties such as high strength; low weight; good dimensional stability; excellent tearing, cutting, and fatigue resistance; thermal stability; and flame resistance. Thus, the fabrics are uniquely qualified for a variety of special load-bearing elements in engineering applications of the material such as ballistic protection materials, inflatable structures, and the impact attenuation system in aerospace vehicle-recovery technology. The strong skin of the fabric/foam composite structure is made of a thin layer composite consisting of Kevlar fabric and polyurethane resin. Two kinds of commonly employed aramid fibers, Kevlar 29 and Kevlar 49, are presently used in the skin construction. The fabrics have a plain weave structure with a weight of 7.0 oz/sq yd (0.24 kg/m^2) and 10.0 oz/sq yd (0.34 kg/m^2), respectively. Fiber volume fractions along the warp and filled directions in the composite skin are both about 15 percent. Young's moduli of the composite skin have been determined, both experimentally and theoretically,[9] giving values of about 1.35×10^6 psi (9.31×10^7 Pa) and 2.85×10^6 psi (1.96×10^{10} Pa) for the Kevlar 29 and Kevlar 49 fabric composite skins, respectively. These material properties will be used directly in the present analysis.

In contrast to the ductile nature of certain polymers, the polyurethane foam core tends to exhibit brittle behavior and has very low strength in tensile. However, in compression, the foam has constitutive behavior similar to ductile polymers with an apparent yield stress, large elongation, and relatively high ultimate tensile strength. The apparent yield stress is considered generally to be related to the collapse of the cell structure in the foam. Although several theories for evaluating the elastic modulus of the foam have been proposed, the Kerner equation and the modified Halpin-Tsai equations[10] seem to give the most favorable results when compared to the experiments. For the low-density foams used in this study, elastic moduli of the foams have been found to be related to the density of the foam by a linear relationship.

Figure 14 shows the experimentally determined, static stress/strain behavior of two kinds of polyurethane foams with different densities (2 and 4 lb/cu ft [32 and 64 kg/m^3]). The nonlinearity in the figure is quite obvious as strains exceed 2 percent. For the convenience of the analytical development, the experimental data were fitted into continuous curves by a best least-square, curve-fitting technique to give constitutive equations. In the elastic range of foam deformation, Young's moduli of the foams have been determined to be 850 psi and 2400 psi (5.86×10^6 Pa and 1.65×10^7 Pa), respectively, for the low and high density foams. In the inelastic range, the constitutive relations of the foams have the following forms:

$$\sigma = [48. + 260. (|\epsilon| - 0.02)^{0.7}] \ \mathrm{sgn}(\epsilon) \qquad \text{[Eq 47a]}$$

for the 4 lb/cu ft (64 kg/m^3) polyurethane foam, and

$$\sigma = [17. + 47.2 (|\epsilon| - 0.02)^{0.42}] \ \mathrm{sgn}(\epsilon) \qquad \text{[Eq 47b]}$$

[9] M. W. Wardle, Textile Research Laboratory, E. I. Dupont de Nemours & Company, Wilmington, DE, private communication (1979).

[10] G. J. Fallick, H. J. Bixler, R. A. Marsella, F. F. Garner, and E. M. Fettes, *Modern Plastics*, Volume 45, No. 5 (1968), pp 143-154; L. E. Nielsen, *Mechanical Properties of Polymers and Composites*, Volume 2 (Marcel-Dekker Inc., New York, 1974).

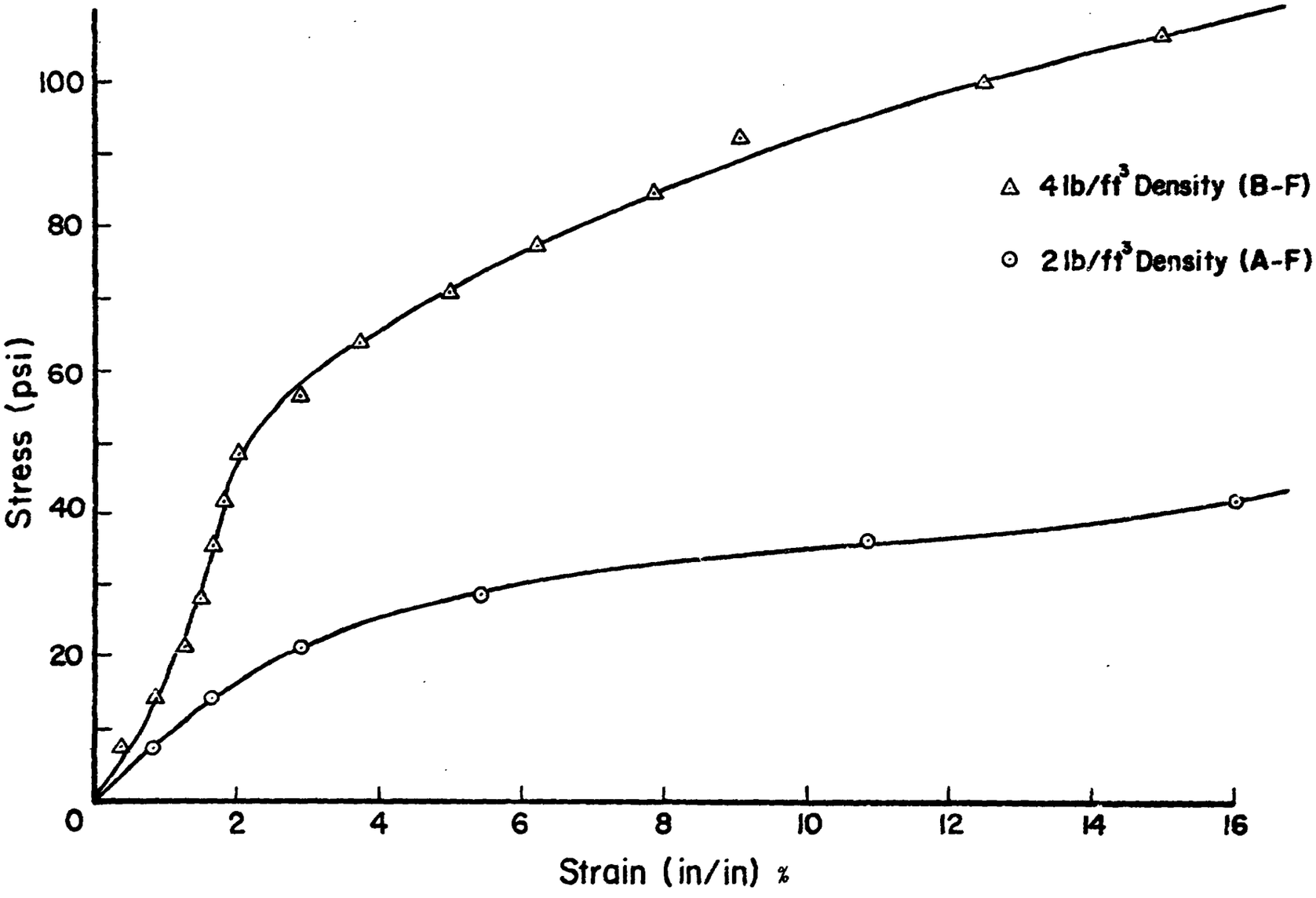

Figure 14. Stress/strain behavior of polyurethane foams with two different densities.

for the 2 lb/cu ft (32 kg/m^3) foam. It should be noted that foams are generally anisotropic because gravity and restraint effects during the foaming process tend to elongate the foam cells in the transverse direction. Thus, it is more difficult to collapse the cell structure in the thickness direction than in the longitudinal direction. The curve extends to exhibit higher elongation, and then the stress rapidly increases after the cell wall has collapsed, which is not shown in the figure.

5 RESULTS AND DISCUSSION

The foam-filled fabric/urethane skin composite cylinder of length 3L (L = 2 ft [.607 m]) and diameter $d_m \cong$(dm = 6 and 12 in. [152 and 305 mm]) subjected to four-point bending, as shown in Figure 9, is considered. Two kinds of fabric material, i.e., Kevlar 29 and Kevlar 49, are used in the skin. The Kevlar fabric/urethane skin has a thickness of about 0.012 to 0.015 in. (0.3048 to 0.3810 mm). The mechanical properties are discussed in the previous section. Two kinds of low density polyurethane foam (2 and 4 lb/cu ft [32 and 64 kg/m^3]) are used as the core material in the composite construction. The foams have very low elastic moduli and deform rapidly into nonlinear range (Figure 14). It is found that the Kevlar fabric/urethane skin bonds very well with the core material. Thus, for each composite beam geometry, four different cases are to be studied. In a four-point bending test, the load P increases continuously, and deflection of the composite cylinder is recorded. Initial elastic deformation of the beam and subsequent local buckling (wrinkling) of the skin are examined by the methods of analysis described in Chapter 3. Progressive extension of the wrinkling portion in a beam section until total failure of the composite by tensile fracture of the skin is determined quantitatively by the nonlinear step-iterative solution scheme mentioned earlier. Analytical solutions for each case are compared with experimental results to ensure the validity of the analyses and to assess the accuracy of the results.

Accuracy and Convergence of Solutions

Accuracy and convergence of present solutions obtained from the aforementioned nonlinear analyses have been examined by solving problems whose solutions are available in the literature and by comparing present analytical results with experimental data. The nonlinear deformation of a cantilever beam (Figure 15) for which plastic behavior of von Mises type is assumed, is chosen here. This problem is attacked by the present step-iterative solution scheme. Figure 16 shows the currently calculated load-deflection curve and the result obtained from Zienkiewicz.[11] As is expected, as the collapse load is approached, progressively large numbers of iterations are required. The two results appear in excellent agreement with each other. The convergence of solutions for nonlinear problems depends on the selection of load increments and the degree of discretization (i.e., number of elements). Figure 17 illustrates graphically the rate of convergence of present solutions by plotting the number of elements vs. the deflection and the curvature at the end of the center line of the deformed beam. It is observed that an error of about 0.1 percent in the solution can be achieved by using 18 elements or more in the present analysis. This example gives important information concerning the discretization of the continuum in the present study. All subsequent analyses for various kinds of foam-filled composite cylinders use numbers of elements which will guarantee an accurate solution within 0.1 percent.

Prediction of Deformation and Local Buckling of Various Fabric/Urethane Foamed Composite Cylinders

The currently established methods are now used to examine actual deformation of the composite cylinders under four-point bending. Solutions have been obtained for the cases of various combinations of materials and geometrical variables. Figures 18, 24, 29, and 35* give both predicted and experimentally observed load-deflection curves of the 12-in. (0.3048-m)-diameter composite beams containing different combinations of fabric/urethane skins and polyurethane foams. Figures 37, 39, 43, and 47 provide similar information for the 6-in. (152-mm)-diameter composite cylinders with various material properties and geometric variables. Open circles in the figures represent experimental data directly determined from the tests. Solid lines indicate the response of the composite beams predicted by the present nonlinear analysis with transverse shear deformation and local

[11] O. C. Zienkiewicz, *The Finite Element Method in Engineering Science* (McGraw-Hill, 1971).

*The appearance of nonsequential figure numbers in the text is intentional. The grouping of basic data figures followed immediately by supporting analytical figures accounts for the arrangement.

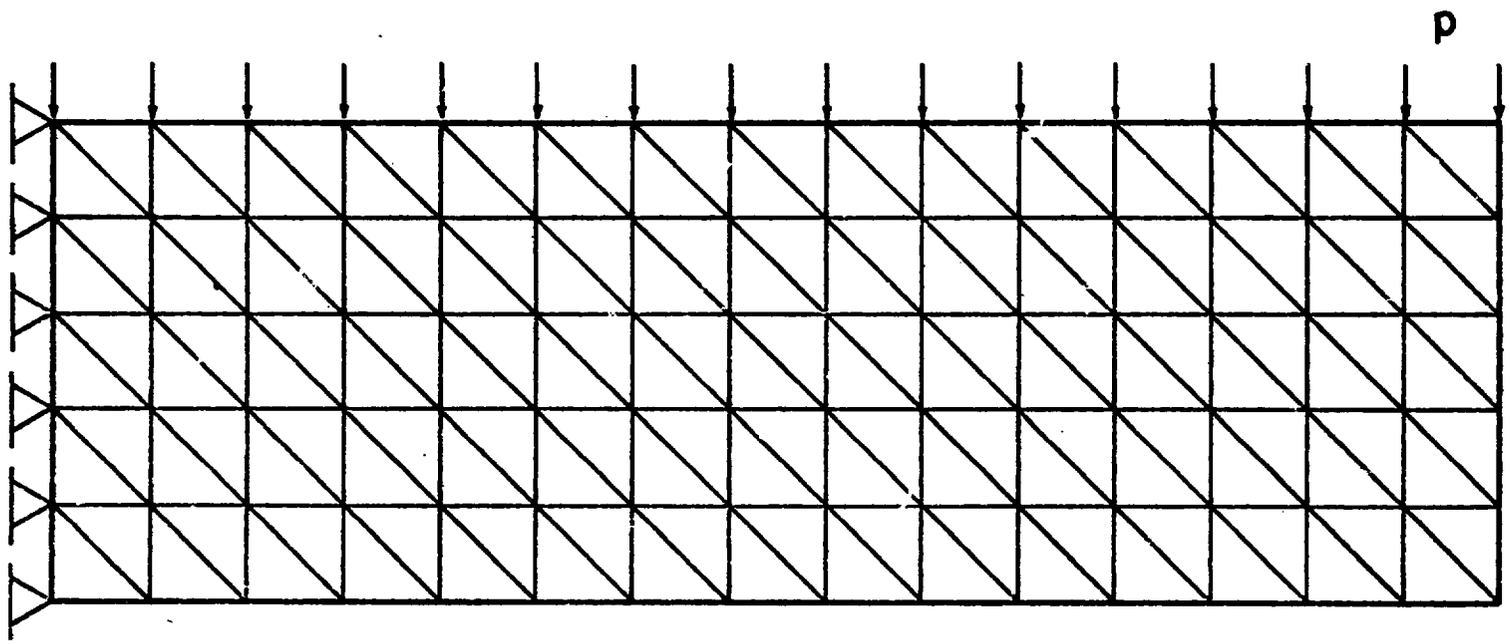

Figure 15. Test case – two-dimensional elastic-plastic deformation of a cantilever beam.

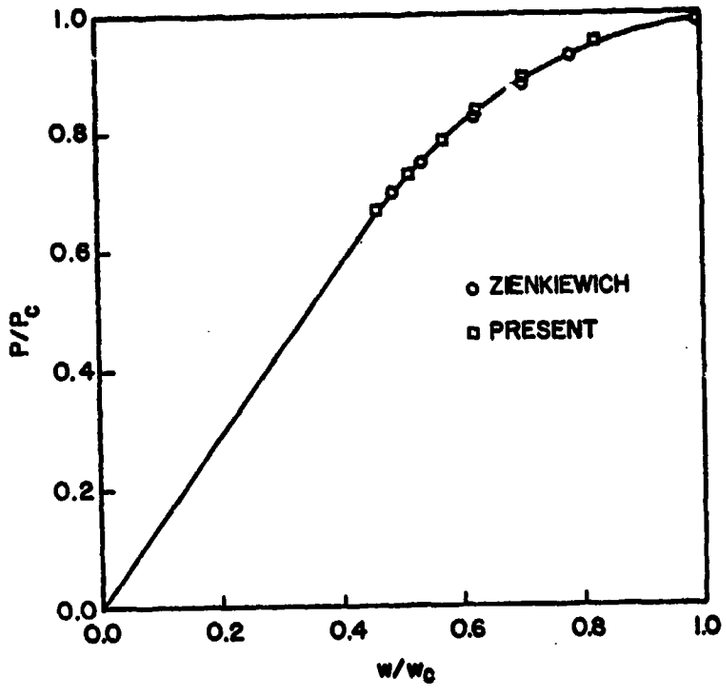

Figure 16. Deflection at the end of the beam vs increasing load.

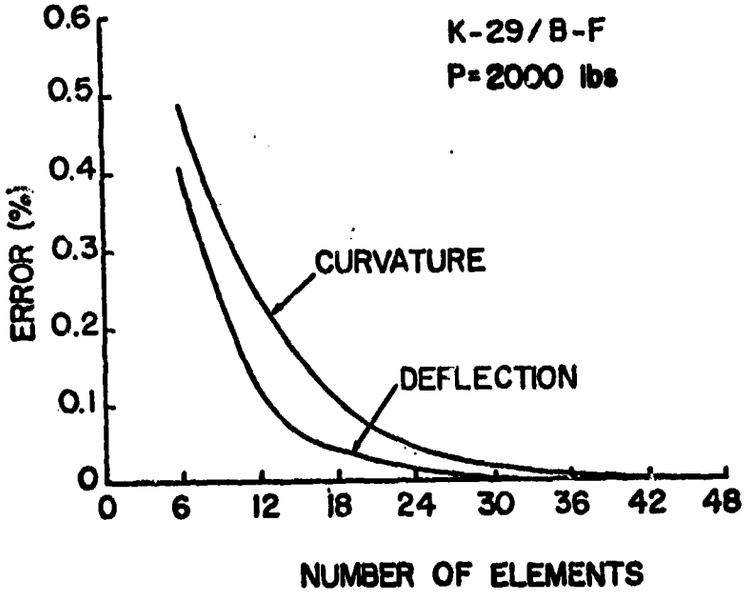

Figure 17. Accuracy and convergence of the nonlinear FEM analysis.

buckling of their skin included in the formulation. These figures have shown that the analytical predictions provide accurate results for almost all cases as compared with the experimental data when the nonlinear behavior of the core, the shear deformation of the soft foams, and the local buckling of the Kevlar fabric/urethane skin are properly considered in the analysis. The local buckling of the thin composite skin starts at a rather low load level and has also been determined by the analysis. It is observed that the wrinkling load P_b is related to the elastic moduli of both the core and the skin materials and that the core material has a greater effect on the local buckling than that of the composite skin. For example, the wrinkling load for the composite beam of Kevlar 49 fabric/4 lb/cu ft (64 kg/m^3) urethane foam is nearly twice as much as that of Kevlar 49 fabric/2 lb/cu (32 kg/m^3) urethane foam composite.

Effects of Shear Deformation

One of the most important problems investigated in the present study is the significance of shear deformation and its effects on the overall deflection of the composite cylinder. In a four-point bending test, total deflection of the beam may be conceived as composed of three components, caused by axial stretching, bending, and shear strains. Shear deformation, usually considered negligibly small in conventional structures, has been observed to be very appreciable in the foam-filled composite subjected to transverse loading.[12] This phenomenon becomes increasingly pronounced after the fabric/urethane skin starts wrinkling. It is extremely significant in the later stage of the beam deformation, when a large portion of the core section is strained into the nonlinear range. Present results have shown that shear deformation in the foam-filled thin skin composite plays an extremely important role in governing the overall response of the composite structure. The shear effects have to be considered in the formulation and analysis of composite cylinders. Failure to include the shear deformation in the analysis will result in a significant error in the final results. Figures 18, 24, and 29, for example, give quantitative information of the effects of shear deformation. It has been found that shear deformation contributes to about half of the total deflection of the cylindrical composite beams during the entire loading history. If not properly taken into account in the study, the predicted load-deflection curves will deviate from the actual experimental results by a significantly large amount. In fact, it has been observed that if the shear deformation is not included, it will not be possible to predict the actual response of the composite for any of the cases, regardless of whatever other complications are included in the formulation.

Core Stresses and Nonlinear Effects

When stresses in the composite cylinder are built up during loading, especially after local buckling of the skin, the core material starts to pick up more loads under increasing external loads. Nonlinear deformation in the foamed core section gradually becomes very significant. The development of core stresses can be calculated precisely by the present nonlinear solution scheme. Figures 19 through 23, 26 through 28, 30 through 34, 40, 41, 42, 44, 45, and 46 present quantitative information of the increasing core stresses from relatively small and linear distributions in the initial stage to highly nonlinear ones in the later stage of deformation. The nonlinear behavior of the core affects the total deformation of the cylindrical composite beam, as can be illustrated in the predicted load-deflection curves for various cases (Figures 18, 24, 35, 37, 38, 43, and 47. It is observed that deviations of deflection from linearity become increasingly significant so that it would be impossible to obtain an accurate prediction of deformation if the nonlinear effects of the core are not included in the analysis.

Progressive Extension of Wrinkling and Compressive Zones in Composite Sections

It has been discussed in the previous section that when local buckling of the thin Kevlar fabric/urethane skin starts, the compressive load-bearing area in the skin begins to decrease and the compressive zone in the core begins to increase so that the equilibrium condition still can hold. As loading continuously increases, progressive extension of the wrinkling and compression zones continues. The reduction of the load-bearing domain in the strong skin and the gradual increase of the compressive loading area in the core are one of the unique features in the deformation and failure behavior of the deployed foam-filled composite. The direct consequence of the extension of the damaged and compressive zones causes the simultaneous shift of the neutral axis y^* and the damage boundary y_b. Thus, y^* shifts from its initial state $y^* = 0$ to $y^* < 0$ as y_b extends from $y_b = \frac{d_o}{2}$ to $y_b > \frac{d_o}{2}$ when $\sigma(f) > \sigma_b$. Both y^* and y_b move downward during the extension of the buckling and compression

[12] F. H. Wittmann, Stevin Report 10-76-5, Stevin Laboratory for Mechanics, Structures and Materials, Delft University of Technology, The Netherlands, 1976.

zones. The amounts of their extension depend on $E^{(s)}$, $E^{(f)}$ and $G^{(f)}$, and on the nonlinear deformation of the core material which can be determined exactly from the present analysis. Figures 19, 21, 25, 30, 36, 38, 44, and 48 give quantitative information of the distances for both y^* and y_b during the entire loading history. In general, it has been observed that the extension of y_b is much larger than that of y^*. For example, the shift of y_b in a Kevlar 49 fabric/4 lb/cu ft (64 k/m^3) polyurethane foam has a value about half of the diameter of the beam, while y^* shifts only less than one tenth of the cylinder diameter, when P = 2000 lb (909 kg).

Additional Remarks

While the present analyses provide accurate means of predicting nonlinear deformation and local buckling of composite cylinders subjected to four-point bending, several material and geometric complexities have not been considered. These may include the anisotropy of the foams and fabrics, the heterogeneity of the core material and the fabric/urethane composite skin, and the geometric nonlinearity caused by large strains developed in the core. Excessive creep of the foamed core under sustained loading has also been noticed, but is not included in the present study. Effects of these complexities on deformation and failure behavior of the composites have not yet been fully explored. Further investigation in these areas should be of significant assistance in a better understanding of the fundamental behavior of the material and will enhance the current capacity of analyzing and predicting more complicated foam-filled composite structure problems.

6 CONCLUSIONS AND RECOMMENDATIONS

Based on the analytical formulation developed in Chapter 3 and the results obtained in Chapter 5, the following conclusions may be drawn:

1. An efficient and accurate method of analysis, formulated by the nonlinear finite element method and local elastic stability theory, has been developed successfully for studying the high-strength fabric/foam composite.

2. Deformation of the cylindrical composite structural element and progressive local failure behavior of the load-bearing skin in the composites with various high-strength fabric materials and core foams can be predicted accurately using the present method of analysis. These results have been confirmed by experimental data.

3. Transverse shear effects, usually considered to be negligibly small in conventional structural members, are shown to play an extremely important role in the overall deformation of the composite and the local failure of the skin. They should be incorporated into the formulation to provide an accurate analysis and prediction.

4. Local buckling (or wrinkling) of the load-bearing composite skin is found to occur at a very low loading level and to initiate nonlinear deformation of the composite in the present four-point bending of the composite cylinder.

5. The nonlinear constitutive relationship of the core material has been observed to significantly affect the deformation and local failure of the composite. This is especially true at the later stage of composite deformation.

6. Progressive extension of the failure zone in the skin causes continuous redistribution of internal stresses in the composite. Direct consequences of this progressive failure are manifested by the reduction of the load-bearing cross-sectional area of the skin and the progressive extension of the compressive domain in the core, which, in many cases, are so significant that the neutral plane is shifted almost to the lower skin.

Based on the experimentally observed and analytically predicted performance, it is recommended that:

1. The high-strength fabric/foam composite system be used as a load-bearing element in a certain class of structures.

2. The currently developed analytical method for predicting the nonlinear deformation and progressive failure of the composite be used in the analysis and design of the composite structural elements.

3. The foam-fabric composite material identified in this study be investigated further to resolve such features as ideal section design, foam density, and fabric design. The composite appears to offer an excellent means of constructing low design load structures but further study is needed in joint design, fastening performance, and component processing techniques.

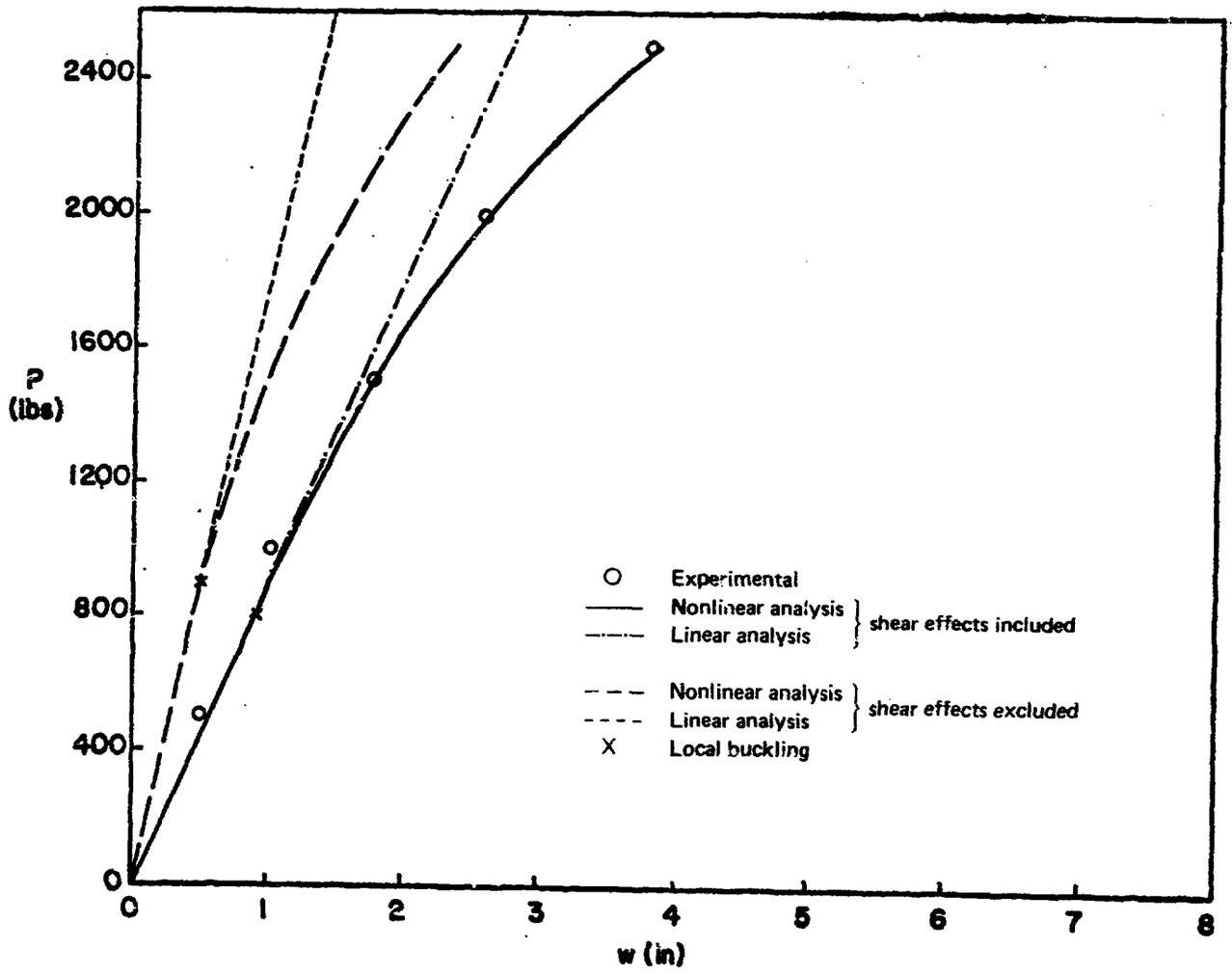

Figure 18. Deflection of central plane (at $z = 0$) in deployable composite cylinder subjected to continuously increasing load (Kevlar 49 fabric/urethane skin and B-F foam; d = 12 in.).

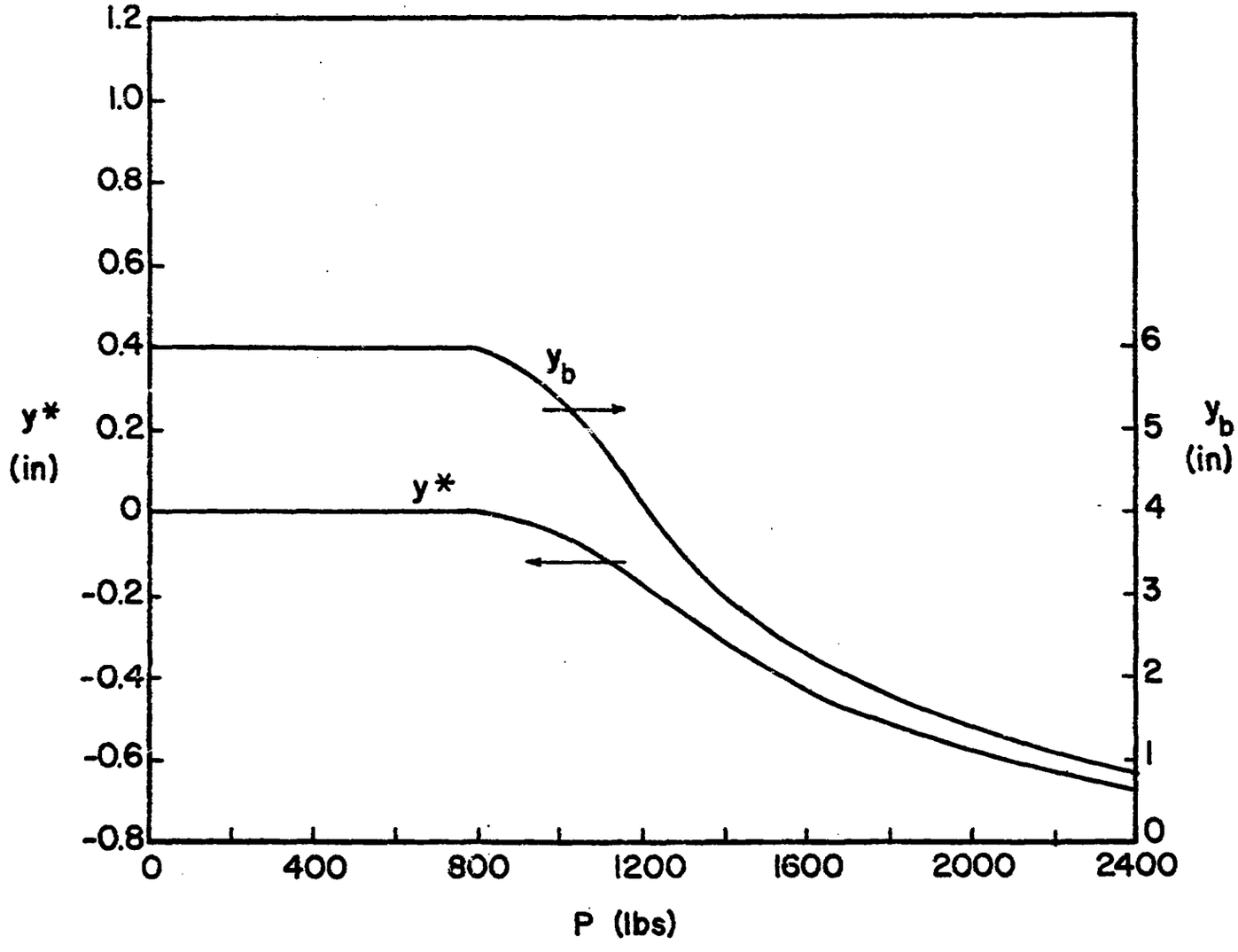

Figure 19. Extension of local failure zone and shift of neutral axis in composite section at z = 0 (Kevlar 49 fabric/urethane skin, and B-F foam; d = 12 in.).

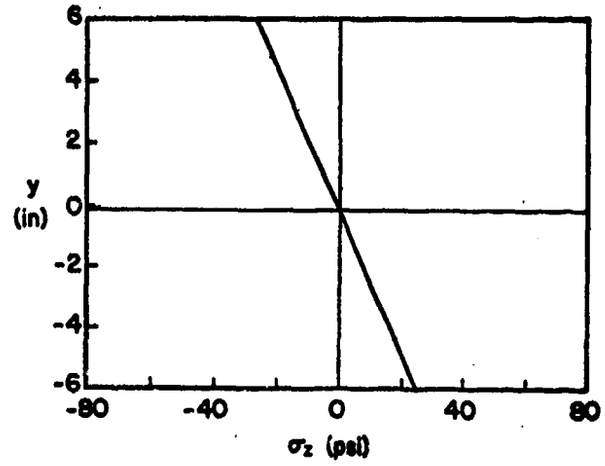

Figure 20. Distribution of σ_z in the core of a composite cross section at z = 0, P = 1200 lb (Kevlar 49 fabric/urethane skin and B-F foam; d = 12 in.).

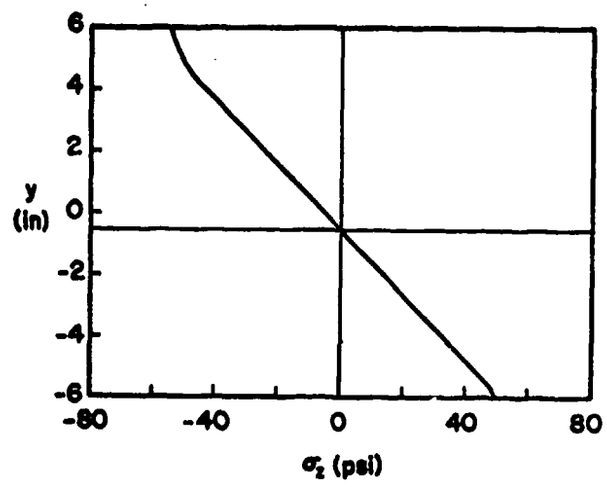

Figure 22. Distribution of σ_z in the core of a composite cross section at z = 0, P = 2000 lb (907 kg) (Kevlar 49 fabric/urethane skin and B-F foam; d = 12 in. [305 mm]).

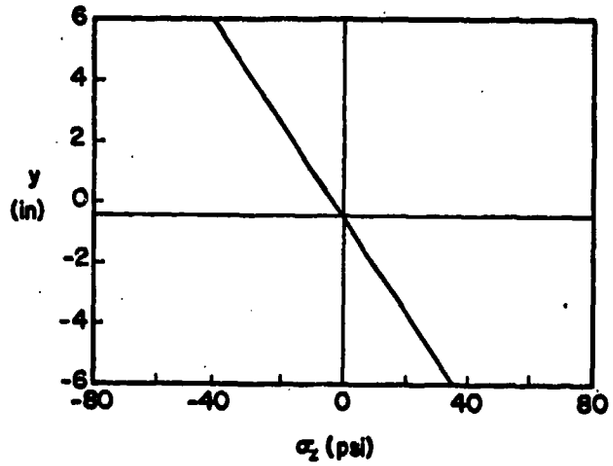

Figure 21. Distribution of σ_z in the core of a composite cross section at z = 0, P = 1600 lb (725 kg) (Kevlar 49 fabric/urethane skin and B-F foam; d = 12 in. [305 mm]).

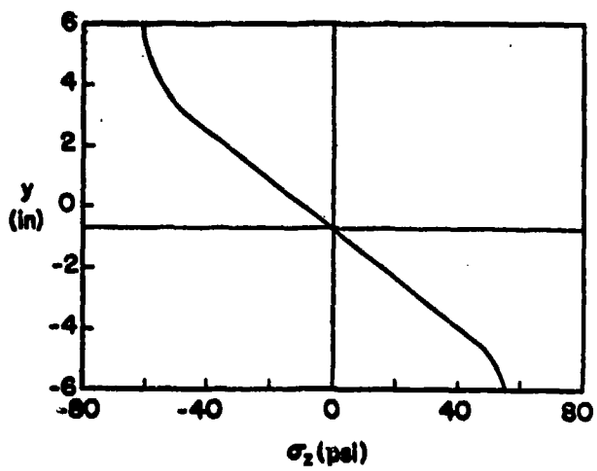

Figure 23. Distribution of σ_z in the core of a composite cross section at z = 0, P = 2400 lb (8 kg) (Kevlar 49 fabric/urethane skin and B-F foam; d = 12 in. [305 mm]).

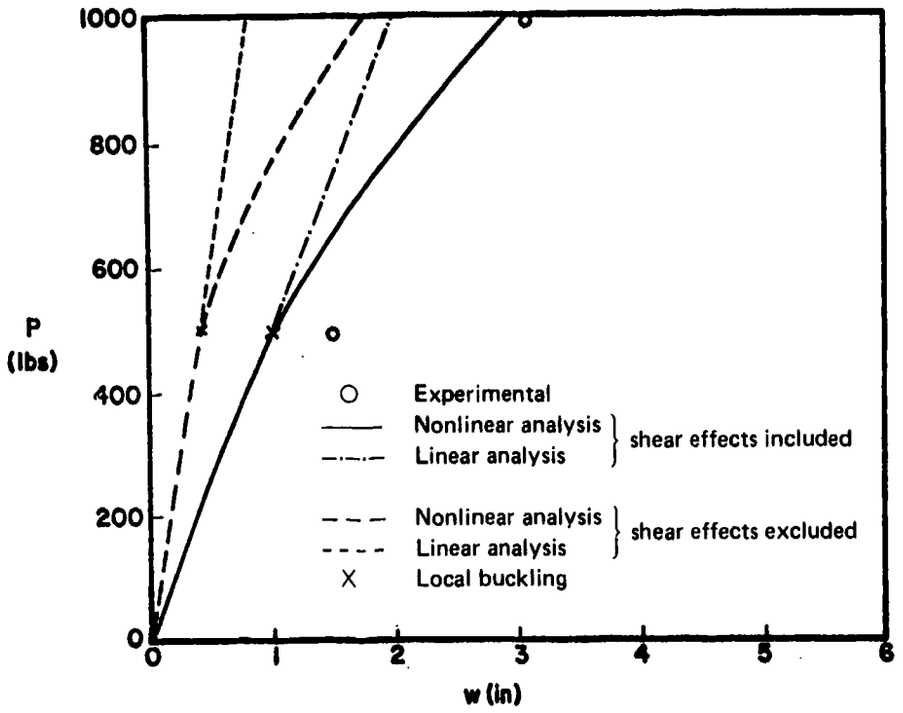

Figure 24. Deflection of the central plane (at z = 0) in deployable composite cylinder subjected to continuously increasing load (Kevlar 49 fabric/urethane skin and A-F foam; d = 12 in. [305 mm]).

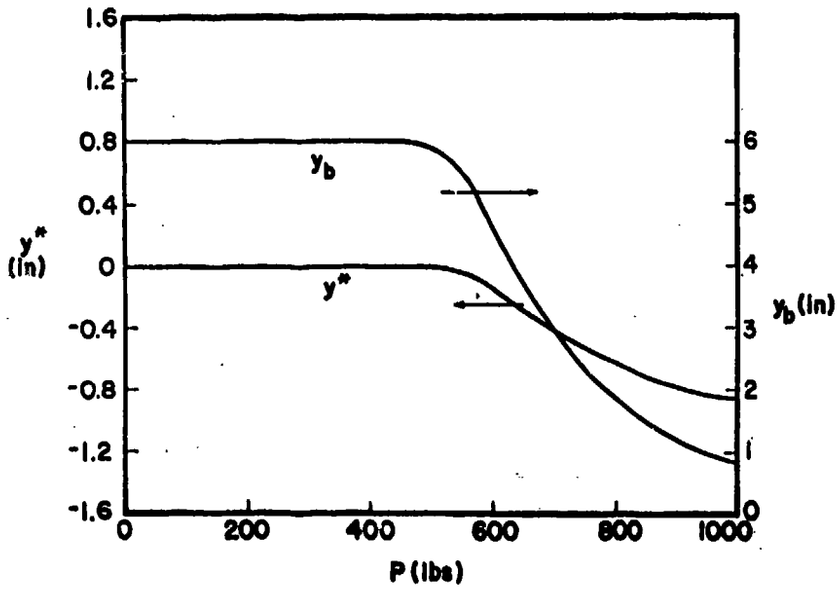

Figure 25. Extension of local failure zone and shift of neutral axis in the composite section at z = 0 (Kevlar 49 fabric/urethane skin and A-F foam; d = 12 in. [305 mm]).

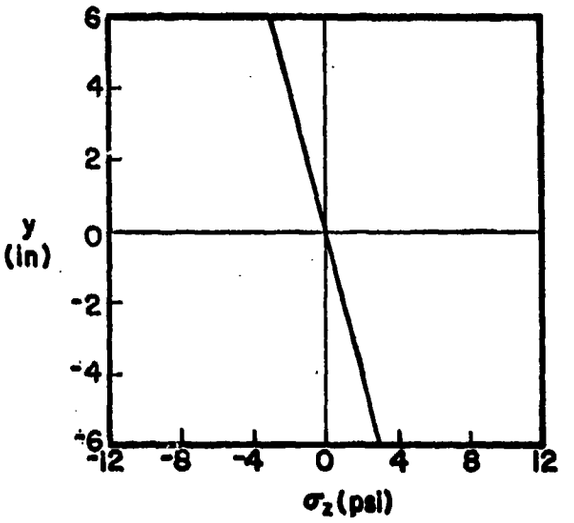

Figure 26. Distribution of σ_z in the core of a composite cross section at z = 0, P = 500 lb (227 kg) (Kevlar 49 fabric/urethane skin and A-F foam; d = 12 in. [305 mm]).

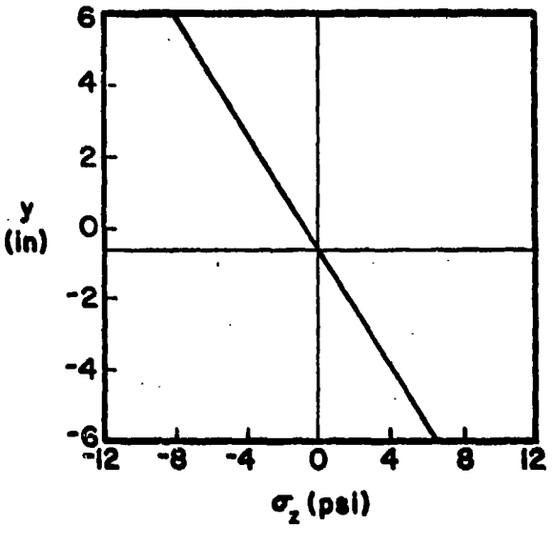

Figure 27. Distribution of σ_z in the core of a composite cross section at z = 0, P = 800 lb (362 kg) (Kevlar 49 fabric/urethane skin and A-F foam; d = 12 in. [305 mm]).

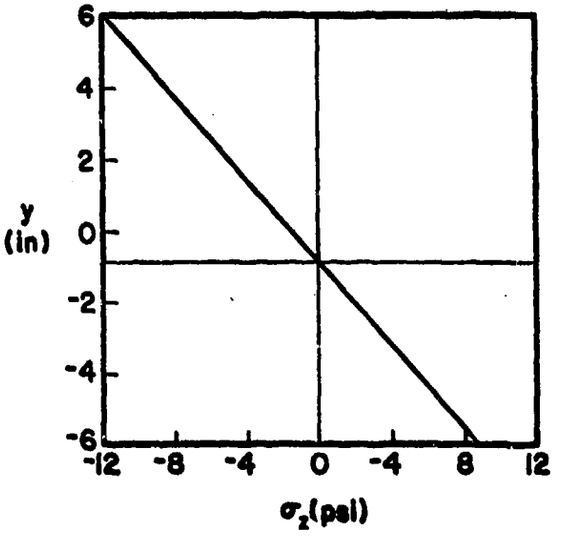

Figure 28. Distribution of σ_z in the core of a composite cross section at z = 0, P = 1000 lb (453 kg) (Kevlar 49 fabric/urethane skin and A-F foam; d = 12 in. [305 mm]).

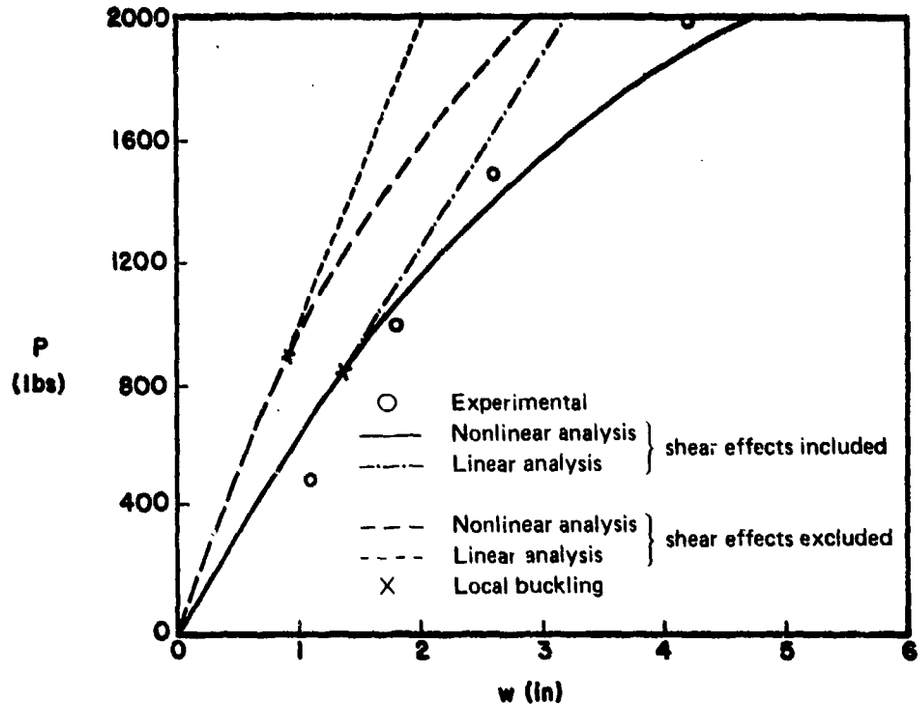

Figure 29. Deflection of central plane (at z = 0) in deployable composite cylinder subjected to continuously increasing load (Kevlar 29 fabric/urethane skin and B-F foam; d = 12 in. [305 mm]).

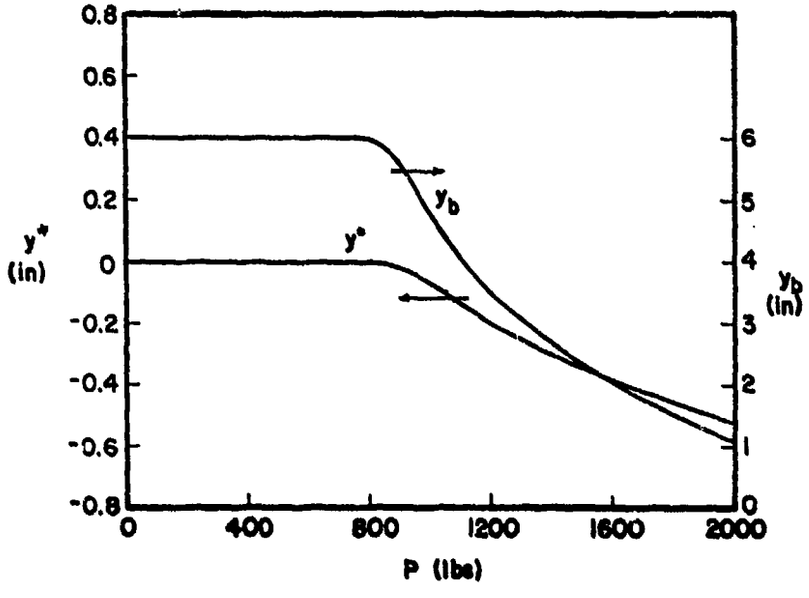

Figure 30. Extension of failure zone in skin and shift of neutral axis in a composite section at z = 0 (Kevlar 29 fabric/urethane skin and B-F foam; d = 12 in. [305 mm]).

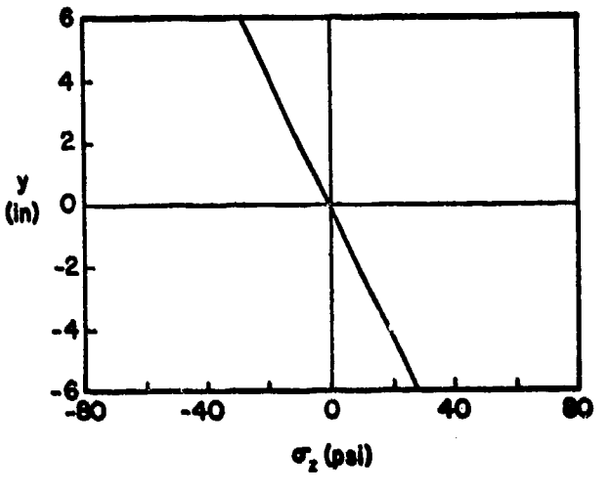

Figure 31. Distribution of σ_z in the core of a composite cross section at z = 0, P = 800 lb (362 kg) (Kevlar 29 fabric/urethane skin and B-F foam; d = 12 in. [305 mm]).

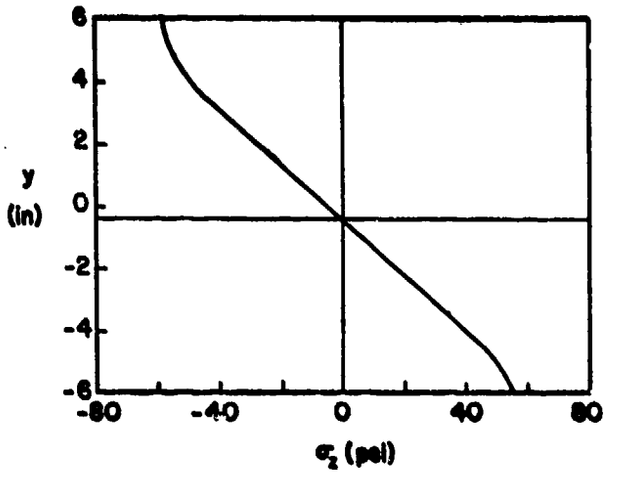

Figure 33. Distribution of σ_z in the core of a composite cross section at z = 0, P = 1600 lb (725 kg) (Kevlar 29 fabric/urethane skin and B-F foam; d = 12 in. [305 mm]).

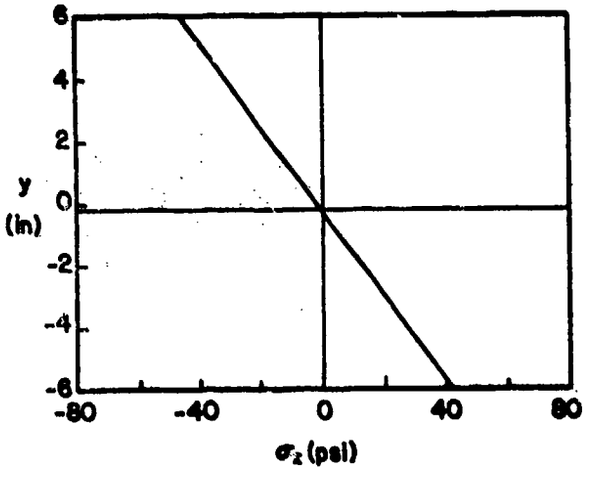

Figure 32. Distribution of σ_z in the core of a composite cross section at z = 0, P = 1200 lb (544 kg) (Kevlar 29 fabric/urethane skin and B-F foam; d = 12 in. [305 mm]).

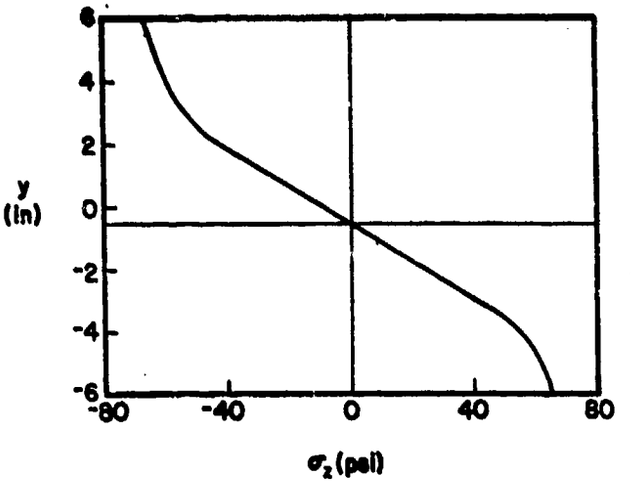

Figure 34. Distribution of σ_z in the core of a composite cross section at z = 0, P = 2000 lb (907 kg) (Kevlar 29 fabric/urethane skin and B-F foam; d = 12 in. [305 mm]).

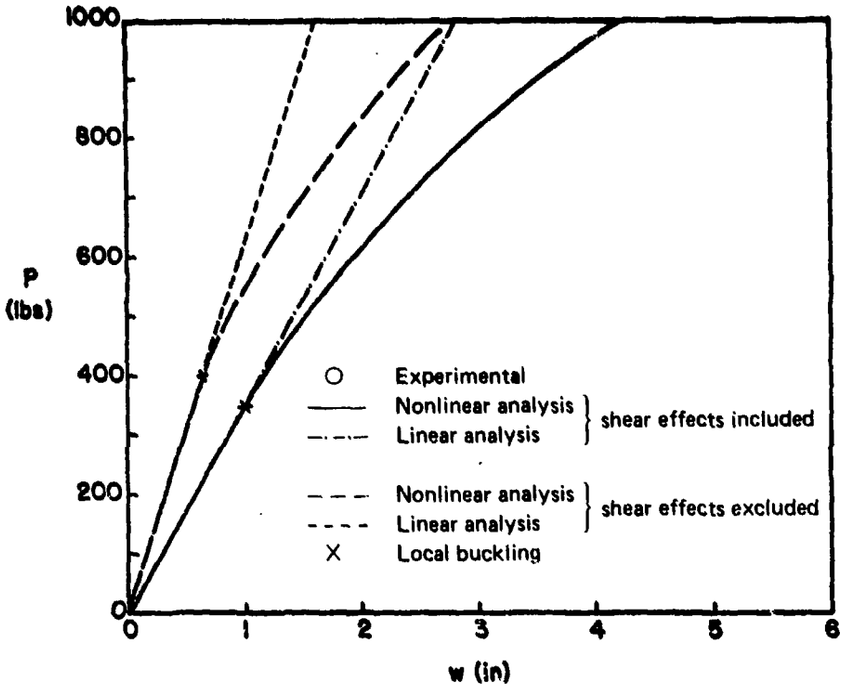

Figure 35. Deflection of central plane (at z = 0) in deployable composite cylinder subjected to continuously increasing load (Kevlar 29 fabric/urethane skin and A-F foam; d = 12 in. [305 mm]).

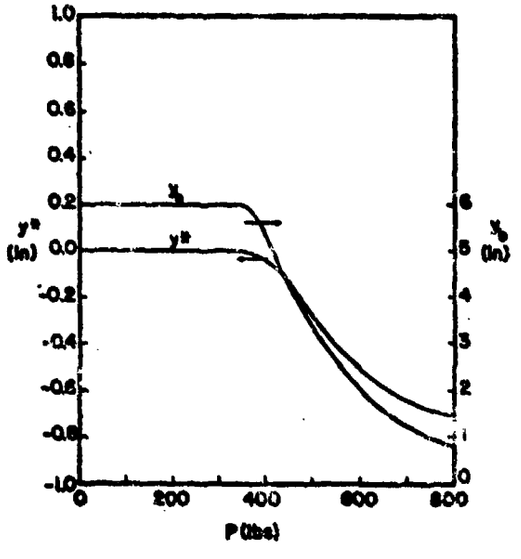

Figure 36. Extension of failure zone in skin and shift of neutral axis in a composite section at z = 0 (Kevlar 29 fabric/urethane skin and A-F foam; d = 12 in. [305 mm]).

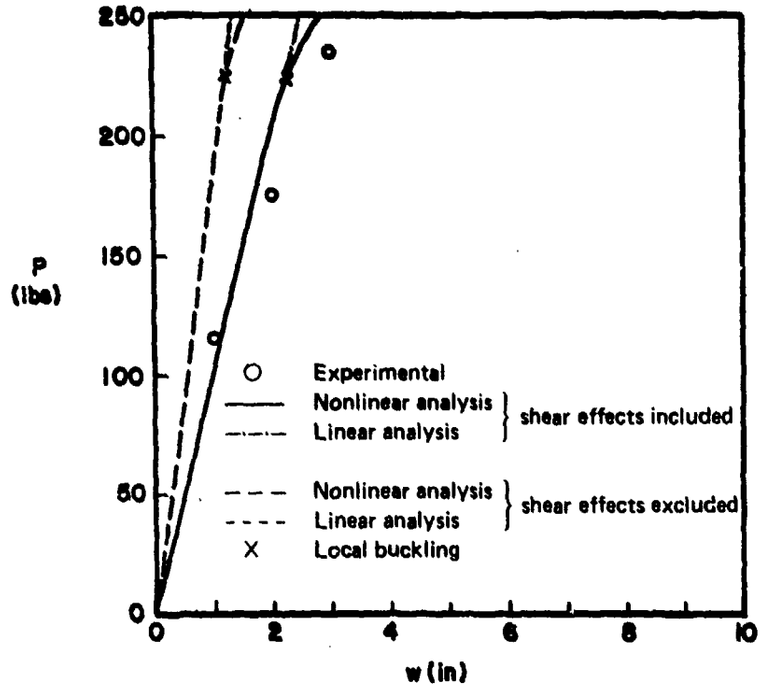

Figure 37. Deflection of central plane (at z = 0) in deployable composite cylinder subjected to continuously increasing load (Kevlar 49 fabric/urethane skin and B-F foam; d = 6 in. [152 mm]).

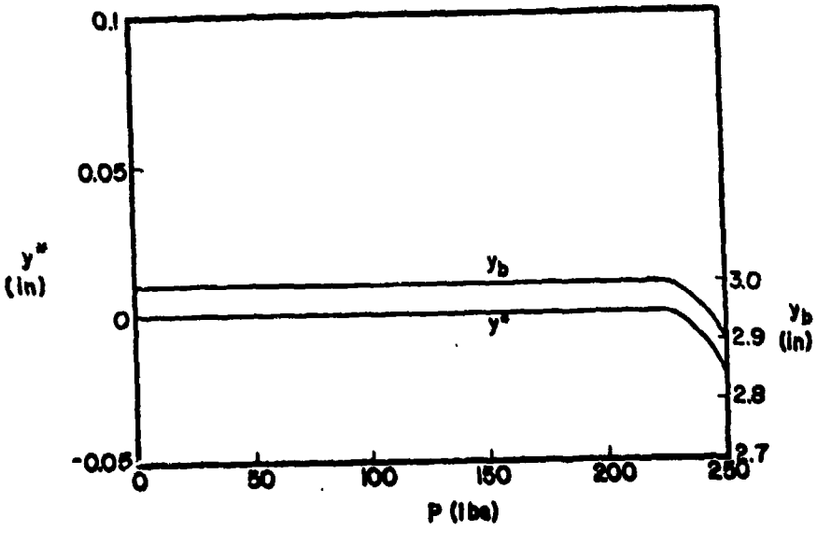

Figure 38. Extension of failure zone in skin and shift of neutral axis in a composite section at z = 0 (Kevlar 49 fabric/urethane skin and B-F foam; d = 6 in. [152 mm]).

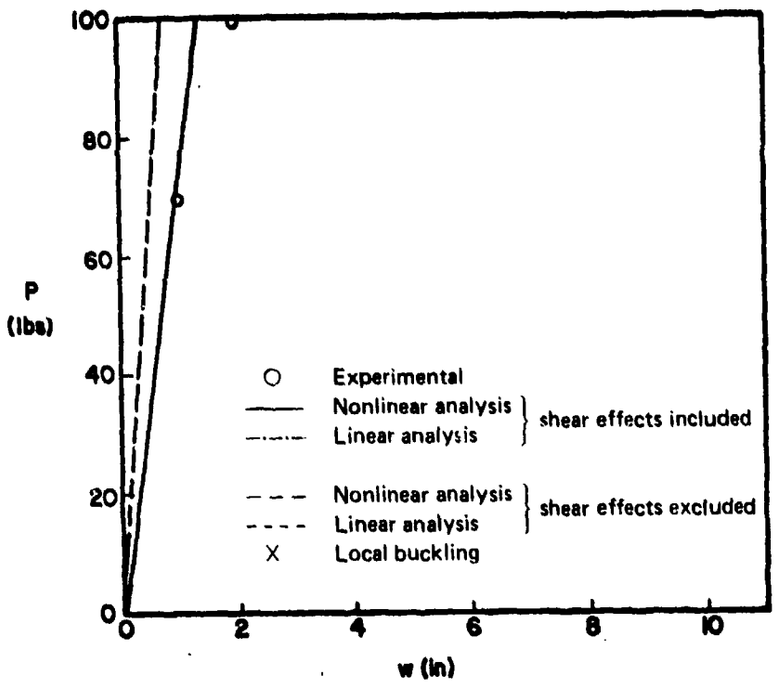

Figure 39. Deflection of central plane (at z = 0) in deployable composite cylinder subjected to continuously increasing load (Kevlar 49 fabric/urethane skin and A-F foam; d = 6 in. [152 mm]).

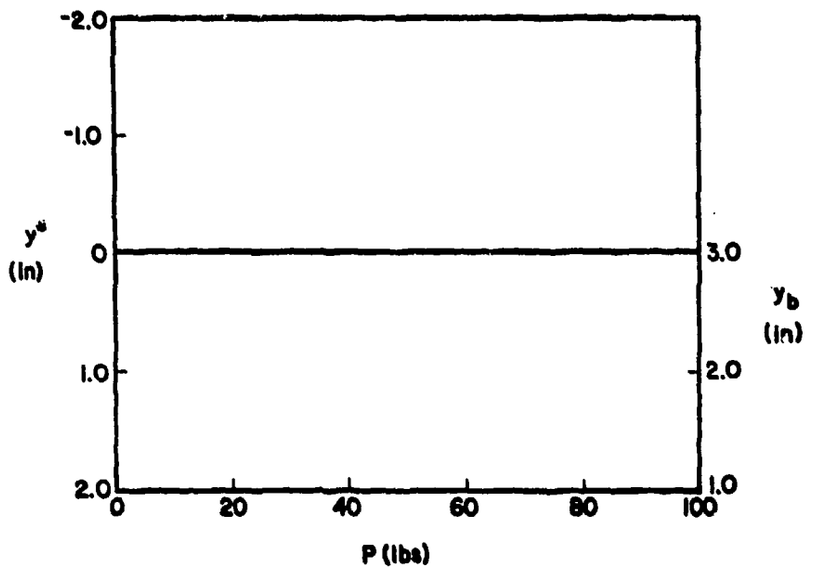

Figure 40. Extension of failure zone in skin and shift of neutral axis in a composite section at z = 0 (Kevlar 49 fabric/urethane skin and A-F foam; d = 6 in. [152 mm]).

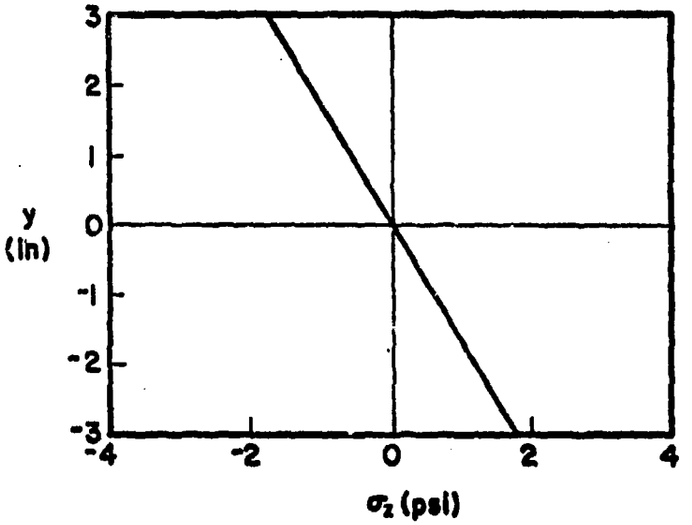

Figure 41. Distribution of σ_z in the core of a composite cross section at z = 0, P = 60 lb (27 kg) (Kevlar 49 fabric/urethane skin and A-F foam; d = 6 in. [152 mm]).

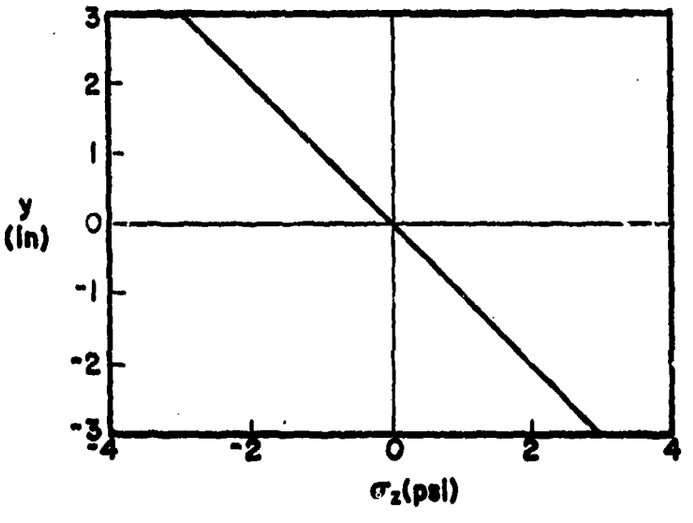

Figure 42. Distribution of σ_z in the core of a composite cross section at z = 0, P = 100 lb (45 kg) (Kevlar 49 fabric/urethane skin and A-F foam; d = 6 in. [152 mm]).

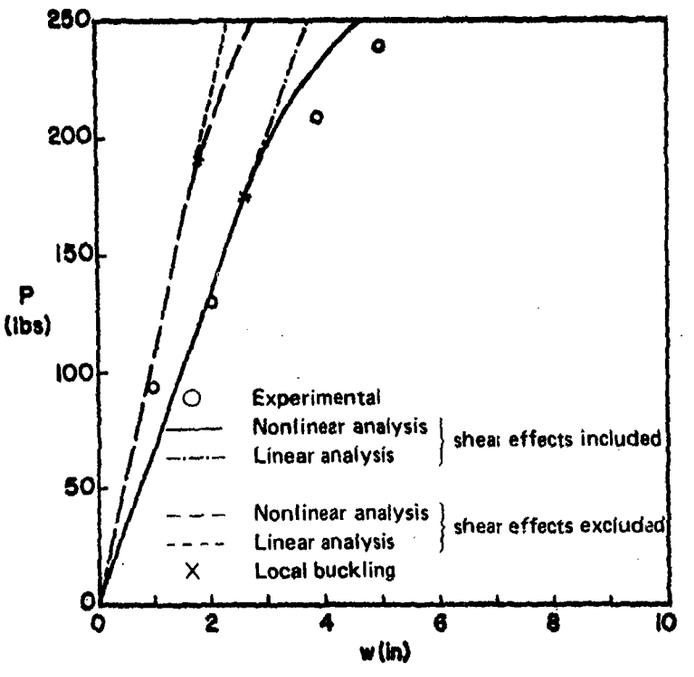

Figure 43. Deflection of central plane (at z = 0) in deployable composite cylinder subjected to continuously increasing load (Kevlar 29 fabric/urethane skin and B-F foam; d = 6 in. [152 mm]).

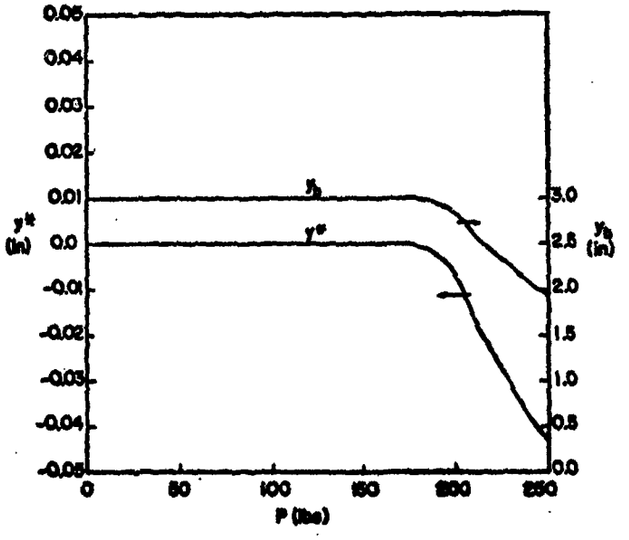

Figure 44. Extension of failure zone in skin and shift of neutral axis in a composite cross section at z = 0 (Kevlar 29 fabric/urethane skin and B-F foam; d = 6 in. [152 mm]).

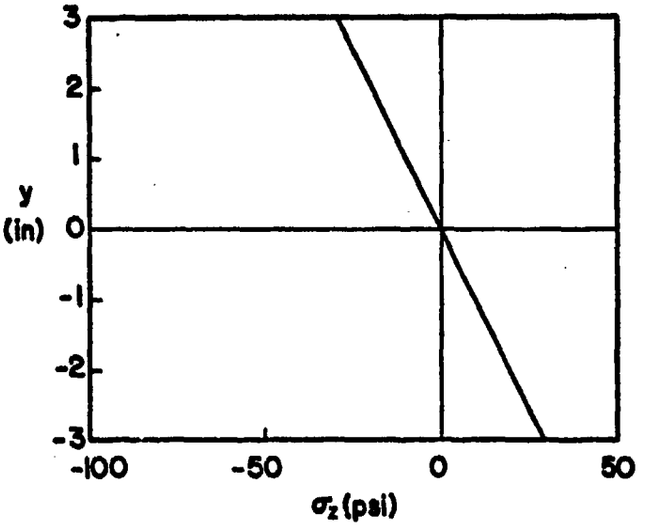

Figure 45. Distribution of σ_z in the core of a composite cross section at z = 0, P = 150 lb (68 kg) (Kevlar 29 fabric/ urethane skin and B-F foam; d = 6 in. [152 mm]).

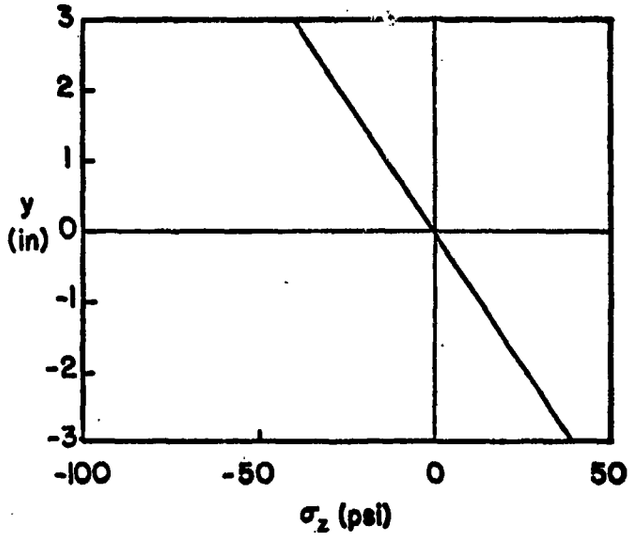

Figure 46. Distribution of σ_z in the core of a composite cross section at z = 0, P = 250 lb (113 kg) (Kevlar 29 fabric/urethane skin and B-F foam; d = 6 in. [152 mm]).

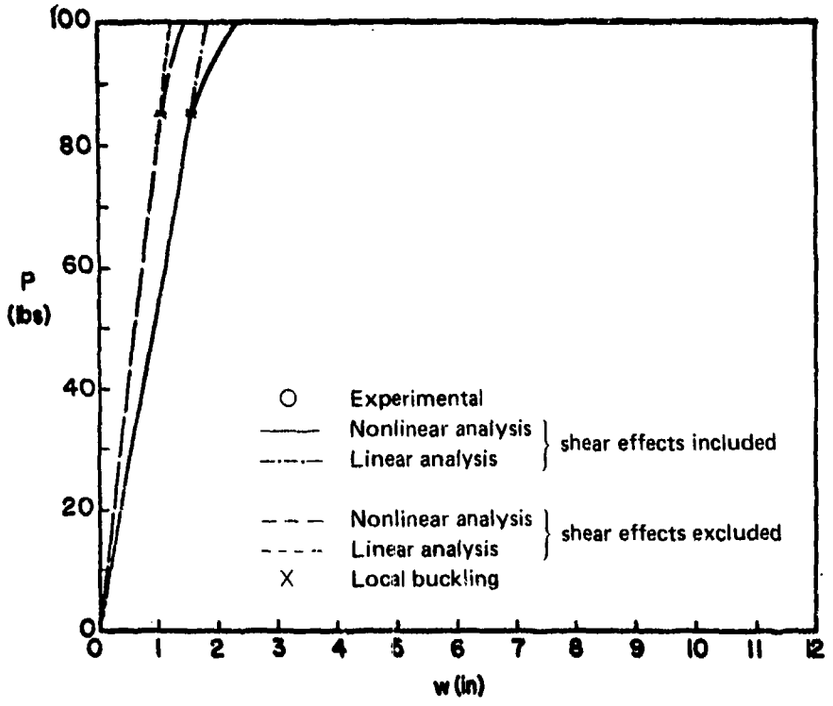

Figure 47. ılection of central plane (at z = 0) in deployable composite cylinder subjected to continuously increasing load (Kevlar 29 fabric/urethane skin and A-F foam; d = 6 in. [152 mm]).

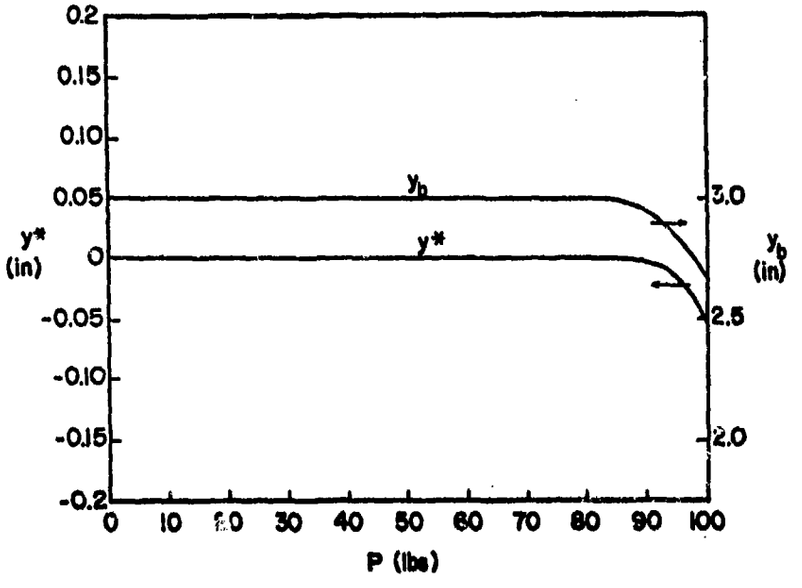

Figure 48. Extension of failure zone in skin and shift of neutral axis in a composite cross section at z = 0 (Kevlar 29 fabric/urethane skin and A-F foam; d = 6 in. [152 mm]).

REFERENCES

Card, M. F., "Trends in Aerospace Structures," *Astronautics and Aeronautics*, Volume 16 (1978), pp 82-89.

Desai, C. S. and Abel, J. F., *Introduction to the Finite Element Method* (Van Nostrand Reinhold Company, 1972).

Eringen, A. C., "Buckling of a Sandwich Cylinder under Uniform Axial Compressive Loading," *Journal of Applied Mechanics*, Volume 18, No. 2 (1951), pp 195-202.

Fallick, G. J., Bixler, H. J., Marsella, R. A., Garner, F. F., and Fettes, E. M., *Modern Plastics*, Volume 45, No. 5 (1968), pp 143-154.

Hagler, T., "Building Large Structures in Space," *Astronautics and Aeronautics*, Volume 14 (1976), pp 56-61.

Mehaffie, S. R., "Foam Impact Attenuation System," *A Collection of Technical Papers, AIAA 6th Aerodynamic Decelerator and Balloon Technology Conference*, Houston, TX, March 5-7, 1979.

Mehaffie, S. R., *Investigation of a Deployable Polyurethane Foam Ground Impact Attenuation System for Aerospace Vehicles (FIAS Tests #1-#48)*, AFFDL-TR-78-145, Volume I (Wright-Patterson AFB [WPAFB], 1977).

Mehaffie, S. R., *Investigation of a Deployable Polyurethane Foam Ground Impact Attenuation System for Aerospace Vehicles (FIAS Tests #49-#91)*, AFFDL-TR-78-145, Volume II (WPAFB, 1978).

Mehaffie, S. R., *State of the Art of Impact Attenuation Concepts for RPV Applications*, AFFDL-TR-76-51 (WPAFB, 1976).

Mindlin, R. D., "Influence of Rotatory Inertia and Shear on Flexual Motions of Isotropic Elastic Plates," *Journal of Applied Mechanics*, Volume 18 (1951), pp 31-38.

Nielson, L. E., *Mechanical Properties of Polymers and Composites*, Volume 2 (Marcel-Dekker Inc., 1974).

Smith, A., *Investigation of a Minimum Time Foam Deployment System*, draft Technical Report (CERL, 1979).

Williams, D., *Sandwich Construction-A Practical Approach for the Use of Designers*, RAE Report No. Structures, 2, M. 2466 (1947).

Wittman, F. H., Stevin Report 10-76-5 (Stevin Laboratory for Mechanics, Structures and Materials, Delft University of Technology, The Netherlands, 1976).

Zienkiewicz, O. C., *The Finite Element Method in Engineering Science* (McGraw-Hill, 1971).

APPENDIX:
ELEMENT STIFFNESS MATRIX k OF THE BEAM

$k_{11} = C_{11}/\ell^2$
$k_{12} = -(12\xi - 6)\, C_{12}/\ell^3$
$k_{13} = -(6\xi - 4)\, C_{12}/\ell^2$
$k_{14} = -C_{12}/\ell^2$
$k_{15} = -C_{11}/\ell^2$
$k_{16} = (12\xi - 6)\, C_{12}/\ell^3$
$k_{17} = -(6\xi - 2)\, C_{12}/\ell^2$
$k_{18} = C_{12}/\ell^2$
$k_{22} = (12\xi - 6)^2\, C_{22}/\ell^4$
$k_{23} = (12\xi - 6)(6\xi - 4)\, C_{22}/\ell^3$
$k_{24} = (12\xi - 6)\, C_{22}/\ell^3$
$k_{25} = (12\xi - 6)\, C_{12}/\ell^3$
$k_{26} = -(6 - 12\xi)^2\, C_{22}/\ell^4$
$k_{27} = (12\xi - 6)(6\xi - 2)\, C_{22}/\ell^3$
$k_{28} = -(12\xi - 6)\, C_{22}/\ell^3$
$k_{33} = (6\xi - 4)^2\, C_{22}/\ell^2$
$k_{34} = (6\xi - 4)\, C_{22}/\ell^2$
$k_{35} = (6\xi - 4)\, C_{12}/\ell^2$
$k_{36} = (6\xi - 4)(6 - 12\xi)\, C_{22}/\ell^3$
$k_{37} = (6\xi - 2)(6\xi - 4)\, C_{22}/\ell^2$
$k_{38} = -(6\xi - 4)\, C_{22}/\ell^2$
$k_{44} = C_{22}/\ell^2 + (1 - \xi)^2\, C_{33}$
$k_{45} = C_{12}/\ell^2$
$k_{46} = (6 - 12\xi)\, C_{22}/\ell^3$
$k_{47} = (6\xi - 2)\, C_{22}/\ell^2$
$k_{48} = -C_{22}/\ell^2 + C_{33}\, \xi\, (1 - \xi)$
$k_{55} = C_{11}/\ell^2$
$k_{56} = (6 - 12\xi)\, C_{12}/\ell^3$
$k_{57} = (6\xi - 2)\, C_{12}/\ell^2$
$k_{58} = -C_{12}/\ell^2$
$k_{66} = (6 - 12\xi)^2\, C_{22}/\ell^4$
$k_{67} = (6\xi - 2)(6 - 12\xi)\, C_{22}/\ell^3$
$k_{68} = -(6\xi - 12)\, C_{22}/\ell^3$
$k_{77} = (6\xi - 2)^2\, C_{22}/\ell^2$
$k_{78} = -(6\xi - 2)\, C_{22}/\ell^2$
$k_{88} = C_{22}/\ell^2 + \xi^2\, C_{33}$

CERL DISTRIBUTION

Picatinny Arsenal
ATTN: SMUPA-VP3

Director of Facilities Engineering
APO New York, NY 09827
APO Seattle, WA 98749

DARCOM STIT-EUR
APO New York 09710

USA Liaison Detachment
ATTN: Library
New York, NY 10007

West Point, NY 10996
ATTN: Dept of Mechanics
ATTN: Library

HQDA (SGRD-EDE)

Chief of Engineers
ATTN: Tech Monitor
ATTN: DAEN-ASI-L (2)
ATTN: DAEN-MPO-B
ATTN: DAEN-MPZ-A
ATTN: DAEN-MPR (2)
ATTN: DAEN-RDL
ATTN: DAEN-ZCP

National Defense Headquarters
Director General of Construction
Ottawa, Ontario K1A0K2
Canada

Div of Bldg Research
National Research Council
Montreal Road
Ottawa, Ontario K1A0R6
Canada

Airports and Const. Services Dir.
Technical Information Reference
Center
KA0L, Transport Canada Buiding
Place de Ville,
Ottawa, Ontario K1A0N8
Canada

British Liaison Officer (5)
U.S. Army Mobility Equipment
Research and Development Center
Ft. Belvoir, VA 22060

Ft. Belvoir, VA 22060
ATTN: ATSE-TD-TL (2)
ATTN: Learning Resources Center
ATTN: Kingman Bldg, Library
ATTN: FESA
ATTN: MAJ Shurb (4)

US Army Foreign Science and
Tech Center
ATTN: Charlottesville, VA 22901
ATTN: Far East Office

Ft. Leavenworth, KS 66027
ATZLCA-SA/T. Wolcott

Ft. Monroe, VA 23651
ATTN: ATEN-AD (3)
ATTN: ATEN-FE-ME
ATTN: ATEN-FE-BG (2)

HQ FORSCOM
ATTN: AFEN-CD
ATTN: AFEN-FE
Ft. McPherson, GA 30330

Ft. Lee, VA 23801
ATTN: DRXMC-D (2)

USA-CRREL

USA-WES
ATTN: Concrete Lab
ATTN: Soils & Pavements Lab
ATTN: Library

6th US Army
ATTN: AFKC-EN

1 Corps (ROK/US) Group
ATTN: EACI-EN
APO San Francisco 96358

US Army Engineer District
New York
ATTN: Chief, Design Br.
ATTN: Library
Buffalo
ATTN: Library
Saudi Arabia
ATTN: Library

US Army Engineer District
Pittsburgh
ATTN: Library
ATTN: ORPCD
ATTN: Chief, Engr Div
Philadelphia
ATTN: Library
ATTN: Chief, NAPEN-D
Baltimore
ATTN: Library
ATTN: Chief, Engr Div
Norfolk
ATTN: Library
ATTN: Chief, NAOEN-M
ATTN: NAOEN-D
Huntington
ATTN: Library
ATTN: Chief, ORHED-F
Wilmington
ATTN: Chief, SAWCO-C
ATTN: Chief, SAWEN-D
Charleston
ATTN: Chief, Engr Div
Savannah
ATTN: Library
ATTN: Chief, SASAS-L
Jacksonville
ATTN: Library
ATTN: Const. Div
Mobile
ATTN: Library
ATTN: Chief, SAMEN-D
ATTN: Chief, SAMEN-F
ATTN: Chief, SAMEN
Nashville
ATTN: Chief, ORNED-F
Memphis
ATTN: Chief, Const. Div
ATTN: Chief, LMMED-D
Vicksburg
ATTN: Chief, Engr Div
Louisville
ATTN: Chief, Engr Div
Detroit
ATTN: Library
ATTN: Chief, NCEED-T
St. Paul
ATTN: Chief, ED-D
ATTN: Chief, ED-F
Chicago
ATTN: Chief, NCCCO-C
ATTN: Chief, NCCED-F
Rock Island
ATTN: Library
ATTN: Chief, Engr Div
ATTN: Chief, NCRED-F
St. Louis
ATTN: Library
ATTN: Chief, ED-D
Kansas City
ATTN: Library (2)
ATTN: Chief, Engr Div
Omaha
ATTN: Chief, Engr Div
New Orleans
ATTN: Library (2)
ATTN: Chief, LMNED-DG
Little Rock
ATTN: Chief, Engr Div
Tulsa
ATTN: Library
Fort Worth
ATTN: Library
ATTN: Chief, SWFED-D
ATTN: Chief, SWFED-F
Galveston
ATTN: Chief, SWGAS-L
ATTN: Chief, SWGCO-C
ATTN: Chief, SWGED-DC
Albuquerque
ATTN: Library
ATTN: Chief, Engr Div
Los Angeles
ATTN: Library
ATTN: Chief, SPLED-F
San Francisco
ATTN: Chief, Engr Div
Sacramento
ATTN: Chief, SPKED-D
ATTN: Chief, SPKCO-C
ATTN: Library, Room 8307
Far East
ATTN: Chief, Engr Div
Japan
ATTN: Library
Portland
ATTN: Library
ATTN: Chief, DB-6
ATTN: Chief, FM-1
ATTN: Chief, FM-2
Seattle
ATTN: Chief, NPSCO
ATTN: Chief, NPSEN-FM
ATTN: Chief, EN-DB-ST

US Army Engineer District
Walla Walla
ATTN: Library
ATTN: Chief, Engr Div
Alaska
ATTN: Library
ATTN: Chief, NPASA-R

US Army Engineer Division
Europe
ATTN: Technical Library
New England
ATTN: Library
ATTN: Chief, NEDED-T
ATTN: Laboratory
ATTN: Chief, NEDCD
Middle East (Rear)
ATTN: MEDED-T
North Atlantic
ATTN: Library
ATTN: Chief, NADEN
South Atlantic
ATTN: Library
ATTN: Laboratory
ATTN: Chief, SADEN-TC
ATTN: Chief, SADEN-TS
Huntsville
ATTN: Library (2)
ATTN: Chief, HNDED-CS
ATTN: Chief, HNDED-M
ATTN: Chief, HNDED-SR
Lower Mississippi
ATTN: Library
ATTN: Chief, LMVED-G
Ohio River
ATTN: Laboratory
ATTN: Chief, Engr Div
ATTN: Library
North Central
ATTN: Librar,
Missouri River
ATTN: Library (2)
ATTN: Chief, MRDED-G
ATTN: Laboratory
Southwestern
ATTN: Library
ATTN: Laboratory
ATTN: Chief, SWDED-MA
ATTN: Chief, SWDED-TG
South Pacific
ATTN: Laboratory
Pacific Ocean
ATTN: Chief, Engr Div
ATTN: FM&S Branch
ATTN: Chief, PODED-D
North Pacific
ATTN: Laboratory
ATTN: Chief, NPDEN-TE

Facilities Engineer
FORSCOM
Ft. Devens, MA 01433
Ft. George G. Meade, MD 20755
Ft. McPherson, GA 30330
Ft. Sam Houston, TX 78234
Ft. Carson, CO 80913
Ft. Riley, KS 66442
Ft. Polk, LA 71459
Ft. Ord, CA 93941
Ft. Campbell, KY 42223
Ft. Hood, TX 76544
Ft. Lewis, WA 98433
Ft. Stewart, GA 31313
TRADOC
Ft. Dix, NJ 08640
Ft. Belvoir, VA 22060
Ft. Monroe, VA 23651
Ft. Lee, VA 23801
Ft. Gordon, GA 30905
Ft. McClellan, AL 36201
Ft. Knox, KY 40121
Ft. Benjamin Harrison, IN 46216
Ft. Leonard Wood, MO 65473
Ft. Chaffee, AR 72905
Ft. Sill, OK 73503
Ft. Bliss, TX 79916
West Point, NY 10996
ATTN: MAEN-E
Ft. Benning, GA 31905
ATTN: ATZB-FE-EP
ATTN: ATZB-FE-BG
CAC&FL (3)
Ft. Leavenworth, KS 66027
AMC
Dugway, UT 84022
USACC
Ft. Huachuca, AZ 85613

AF/PREEU
Bolling AFB, DC 20332

AFESC/PRT
Tyndall AFB, FL 32403

Peterson AFB, CO 80914
HQ ADCOM/DEMUS (M. J. Kerby)

Tinker AFB, OK 73145
2854 ABG/DEEE (John Wall)

Patrick AFB, FL 32925
Base CE Sqdn (James T. Burns)

McClellan AFB, CA 95652
2852 APG/DE (LT David C. Hall)

Little Rock AFB
ATTN: 314/DEEE/Mr. Gillham

AFE, Camp Humphreys
APO San Francisco 96271

US Army R&S Group (EUR)
ATTN: AMXSN-E-RM/R. Quattrone
Box 65
FPO NY 09510

Naval Facilities Engr Command
ATTN: Code 04
ATTN: Code 2013 C
Alexandria, VA 22332

Port Hueneme, CA 93043
ATTN: Library (Code L08A)
ATTN: Morrell Library

Commander (Code 2636)
Naval Weapons Center
ATTN: W. C. Bonner P.E.
China Lake, CA 93555

Defense Documentation Center (12)

Washington, DC
ATTN: Bldg Research Advisory Board
ATTN: Library of Congress (2)
ATTN: Federal Aviation Administration
ATTN: Dept of Transportation Library
ATTN: Transportation Research Board
ATTN: US Govt Printing Office (2)

Engineering Societies Library
New York, NY 10017

HQ, US Army Garrison, Honshu
APO San Francisco 96343

Commander
HQ, XVIII Airborne Corps and
Ft. Bragg
ATTN: AFZA-FE-EE
Ft. Bragg, NC 28307

Commander
HQ, 7th Army Training Command
ATTN: AETTG-DEH (5)
APO New York 09114

Commander
HQ USAEREUR and 7th Army
ODCS/Engineer
ATTN: AEAEN-EH (4)
APO New York 09403

Commander
7th Army Combined Arms Training Center
ATTN: AETTM-HRD-EHD
APO New York 09407

Commander
US Army Engineer Div, Europe
ATTN: Technical Library (3)
APO New York 09757

Commander
V Corps
ATTN: AETVDEH
APO New York 09079

Commander
VII Corps
ATTN: AETSDEH
APO New York 09154

Commander
21st Support Command
ATTN: AEREH
APO New York 09325

Commander
US Army Berlin
ATTN: AEBA-EN
APO New York 09742

Commander
US Army Southern European Task Force
ATTN: AESE-ENG
APO New York 09168

Commander
US Army Installation
Support Activity, Europe
ATTN: AEUES-RP
APO New York 09403

LT Neil B. Hall, CEC, USNR (Code 100)
884-6366
US Navy Public Works Center
Box 6, FPO San Francisco 96651

Air Force Distribution (162)

Investigation of rapidly deployable plastic foam systems. -- Champaign, IL : Construction Engineering Research Laboratory ; Springfield, VA : available from NTIS, 1979.
2v. ; 27 cm. (Technical report ; M-272)

Contents : v.1. System development / by Alvin Smith -- v.2. Nonlinear deformation and local buckling of Kevlar fabric / polyurethane foam composites / by Alvin Smith, S. S. Wang, A. Y. Kuo.

1. Plastics in building. 2. Plastic foams. I. Smith, Alvin. II. Wang, Su Su. III. Kuo, an-Yu. IV. Series : U.S. Army Construction Engineering Laboratory. Technical report ; M-272.